Diversity and origin of quartz cements in continental carbonates: example from the Lower Cretaceous rift deposits of the South Atlantic margin

Pierre-Alexandre Teboul, Christophe Durlet, Jean-Pierre Girard, Ludivine Dubois, Galo San Miguel, Aurélien Virgone, Eric C. Gaucher, Gilbert Camoin

Diversity and origin of quartz cements in continental carbonates: example from the Lower Cretaceous rift deposits of the South Atlantic margin

Pierre-Alexandre Teboul [a, b, c], Christophe Durlet[b], Jean-Pierre Girard[a], Ludivine Dubois[a], Galo San Miguel[a], Aurélien Virgone[a], Eric C. Gaucher[a], Gilbert Camoin [c]

[a] TOTAL CSTJF, Avenue Larribau, F-64018 Pau Cedex, France

[b] Univ. Bourgogne Franche-Comté, CNRS, Biogéosciences UMR6282, F-21000 Dijon, France

[c] Aix-Marseille Université, CNRS, IRD, CEREGE UM34, 13545 Aix en Provence, France

Abstract

Silica precipitation in continental carbonates is a common process occurring during sedimentation and diagenesis. The Lower Cretaceous rift deposits of the South Atlantic equatorial margin, which are intensively explored by petroleum companies, provide good examples of such silicifications in carbonates, exhibiting a wide diversity of petrographic habit of early to late quartz cements. In order to understand the palaeoenvironmental and diagenetic conditions leading to this diversity, we integrated detailed petrography of diagenetic sequences and quartz habit with $\delta^{18}O_{quartz}$ measurements (by SIMS) of individual cements observed in samples from the offshore and onshore basins of the West African margin. The petrographic description highlights the omnipresence of early fibrous microquartz cements exhibiting either length-fast or length-slow habit, in addition to laminated microquartz and micro- or mega-quartz forms. Amongst the isotopic analysis, the $\delta^{18}O_{quartz}$ data show that length-slow cements are generally strongly enriched in ^{18}O ($\delta^{18}O_{quartz}$ ranging from 31 to 37‰ SMOW), whereas length-fast forms show less elevated values

(<32‰ SMOW). The highest $\delta^{18}O_{quartz}$ values for fibrous microquartz are interpreted to reflect precipitation from evaporated meteoric fluids at temperatures >25°C and <100°C. The alkalinity required to favor the precipitation of length-slow fibrous microquartz cements is probably related to fluid/rock interactions with underlying mantel-related or basic volcanic rocks. Such interactions would be in agreement with the recent geodynamic models of the South Atlantic passive margin. The length-fast fibrous microquartz associated with $\delta^{18}O_{quartz}$ values ranging from 27 to 32‰ SMOW, probably reflect precipitation from moderately to non evaporated, fairly neutral to acid, fluids. The partial dissolution of carbonate cements prior to quartz cementations represents the signature of those acidic conditions. We therefore suggest that acidic pH was obtained through fluid/rock interactions with the intermediate to acid volcanic rocks encountered along the palaeohydrological pathway. Other quartz phases, such as the megaquartz cement, exhibit highly variable $\delta^{18}O_{quartz}$ values ranging from 20 to 40 ‰. This variation may reflect significant variation in temperature conditions (between 100 and 200°C) or changes in fluid $\delta^{18}O$ at the small scale. For these populations of non-fibrous quartz cement, the very high $\delta^{18}O_{quartz}$ values may reflect a contribution of fluids that have either suffered strong evaporation or strong water/rock interaction.

Keywords: Quartz; Continental carbonates; Diagenesis; Fluid/Rock interaction; Oxygen isotope; Presalt

1. Introduction

Silicification of continental carbonate rocks is common during sedimentation and early to late diagenetic processes (e.g. Spötl & Wright, 1992; Bustillo, 2010; Alonso-Zarza *et al.*, 2011). The relative commonness of these silicifications likely results from several factors. The first one may be related to the fact that continental carbonates are usually less widespread than marine deposits. Consequently, these deposits may remain connected with their silica-rich

substratum and surrounding catchment, from which alteration potentially provided dissolved silica. This abundance can also be due to potentially high silica contents in lacustrine, palustrine, or sinter settings, in relation to diatoms or as amorphous gels (natural gels in recent settings have only rarely been reported; Ernst & Calvert, 1969; Knauth, 1994; Lynne *et al.*, 2005). Continental carbonate silicifications such as sinters may also occur in volcanic settings, associated locally with hydrothermal activity. Volcanic rocks are likely to release silica during their alteration (Hesse, 1989; Teboul *et al.*, 2017). Finally, silicifications are extensively found in evaporitic settings, such as the Magadi Lake (Kenya; Eugster, 1967, 1969; Eugster & Jones, 1968).

In comparison to marine carbonates, quartz in continental carbonates are petrographically highly diversified. The most representative silica succession associated with cementation and/or replacement of carbonate or silica precursors, is typified by: (1) amorphous silica (opal-A), (2) opal-CT, (3) fibrous microquartz, and (4) megaquartz (Folk & Pittman, 1971; Marin, 2009; Warren, 2016). These sequences are seldom observed in marine carbonates, where epigenesis of micrite/allochems and replacement of evaporite nodules by microquartz constitute the majority of the indexed cherts, with other quartz morphologies occurring preferentially in large voids and fractures (Meyers, 1977; Hesse, 1989). Fibrous microquartz cements precipitating in primary and secondary pores of continental carbonates are very common. However, the context of their precipitation is less studied than megaquartz cements (Marin-Carbonne *et al.*, 2011). Fibrous microquartz cements can form through ageing of previously deposited opaline minerals, or direct precipitation from silica-saturated fluids (Bustillo, 2010). They can be found under length-fast or length-slow forms (Folk & Pittman, 1971; Bustillo, 2010; Warren, 2016). Length-slow fibrous microquartz (or lutecite and quartzine) shows a crystallographic c-axis parallel or inclined by circa 30° to the fibers. Length-fast fibrous microquartz (or chalcedony), shows its crystallographic c-axis

perpendicular to the fibers. This interesting duality has been addressed by Folk and Pittman (1971), who used it to identify environments of precipitation. They suggested that length-fast cements are consistent with neutral to acid pH environments, whereas length-slow forms characterize alkaline environments. So far, the use and interpretation of the length-slow vs. length-fast criteria is mainly based on their petrographic features and their frequent association with evaporitic minerals. A recent approach from Bustillo *et al*. (2017) showed the predominance of length-slow forms in carbonate-evaporite precipitating lakes, and the predominance of length-fast forms in carbonate precipitating lakes. No studies have yet documented whether the isotopic composition of the different fibrous microquartz ($\delta^{18}O_{quartz}$) could potentially help to characterize their conditions of precipitation.

The present study focuses on the Lower Cretaceous deposits of the South Atlantic petroleum provinces (Carminatti *et al.,* 2008; Beglinger *et al.*, 2012; Saller *et al.*, 2016). These deposits are overlain by a thick and extensive upper Aptian salt formation. Consequently, the deposits preceding salt deposition are commonly referred-to as “presalt deposits”. The most commonly prospected reservoir formations include the coquina succession (skeletal carbonate; Thompson *et al.*, 2015), microbialites, spherulites, and calcitic shrubs (radiaxial calcite), and possible hydrothermal carbonates (Terra *et al.*, 2010; Saller *et al.*, 2016; Szatmari & Milani, 2016). These deposits are interpreted as mostly derived from freshwater to hypersaline lakes (Saller *et al.*, 2016). Little information has been published on the diagenesis of the presalt carbonates, and the available literature mainly focused on carbonate cementation and neomorphism (Frixa *et al.*, 2015; Wright & Barnett, 2015; Gindre-Chanu *et al*., 2015, 2016; Saller *et al.*, 2016). Despite the reported occurrence of large-scale quartz replacements and cementations (Wright & Barnett, 2015; Saller *et al.*, 2016; Girard & San Miguel, 2017; Goldberg *et al.*, 2017; Poros *et al.*, 2017) the parameters triggering quartz cementation are still debated. Specific geochemical and crystallographic characterization has

been poorly developed on fibrous microquartz cements, with the exception of few $\delta^{18}O_{quartz}$ values from a single presalt site recently published by Saller *et al.* (2016).

The aim of this paper is to characterize and interpret various silica cements from several sites of the Angola and Congo margins through a combined petrographical and geochemical approach. The objectives of our study were therefore to characterize the petrographic habit of quartz cements, to constrain their relative timing of precipitation, and to characterize their $\delta^{18}O_{quartz}$ signature and the possible correlations with the petrographic characteristics. Finally, our aim was also to understand the relationship between the lithological heritage (i.e. substratum types in the palaeohydrological basins) and quartz precipitation, in light of recent works focused on the geological setting (Comin-Chiaramonti et al., 2011), the geodynamic evolution (Unternehr et al., 2010; Péron-Pinvidic et al., 2015), and the alteration of presalt volcanic substratum (Teboul et al., 2017).

2. Geological setting and studied material

2.1. Structural context

The onshore Namibe, Kwanza, and Lower basins were formed during the Neocomian rifting related to the breakup of Pangea (Pletsch et *al.*, 2001; Szatmari & Milani, 2016). This asynchronous opening in time and space led to the initiation of four segments (equatorial, central, southern, and “Falkland”) bounded by major oceanic fracture zones (Torsvik et al., 2009; Moulin et al., 2010; Beglinger et al., 2012; von Nicolai et al., 2013). The Namibe, Kwanza, and Lower Congo basin are located in the Central Segment, aligned along a north-east to south-west transect, on the Angolan and Congolese coasts (Aslanian et al., 2009, Harris, 2000; Fig. 1A). The Namibe basin is bound to the south by the Walvis Ridge (Fig.

1A), which is a volcanic edifice developed above the Tristan da Cunha plume (Moore *et al.*, 1984; O'Connor & Duncan, 1990). Rifting in the Kwanza Basin started at ≈144-140 Ma, with the onset of seafloor spreading at ≈127-117 Ma (Brice et al., 1982; Teisserenc & Villemin, 1990; Guiraud & Maurin, 1992; Quirk et al., 2013). Following Nürnberg & Müller (1991), seafloor spreading was active south of the Walvis Ridge at ≈126 Ma. According to Dingle (1999), during the early Cretaceous, the Walvis Ridge constituted a regional barrier to the marine conditions prevailing in the south.

According to Beglinger *et al.* (2012), the pre-rift basins are considered as intracratonic sag basins, whereas the syn-rift basins are associated with interior fracture basins, controlled by faulting and subsidence. The rifting led to the development of an extensive system composed of half-graben and horst. From the Berriasian to the Barremian, the fault-controlled subsidence led to the development of several fluvial to lacustrine basins filled from fault shoulders erosion products (Bate, 1999). In the early Aptian, the basins underwent thermal subsidence (sag), leading to the widening of the lacustrine systems and to the erosion of the uplifted fault blocks (Karner & Driscoll, 1999).

Recent studies aimed to establish new and more reliable models of the geodynamic evolution of intracratonic rifting and seafloor spreading (Moulin *et al.*, 2010; Unternehr *et al.*, 2010; Chaboureau *et al.*, 2013; Péron-Pinvidic *et al.*, 2015). They demonstrated a strong dissymmetry along the Angola-Namibe rifted margin, and pointed out that crustal thinning is probably favoured by the expansion of large detachment faults generating upper and lower plate domains (Unternehr *et al.*, 2010; Péron-Pinvidic *et al.*, 2015). Large basins with little subsidence would occur in the lower plate domain, controlled by ductile deformation. Narrow subsiding basins with abrupt margins would occur in the upper plate domain, associated with brittle deformation. These authors have localized the volcanic activity in the upper plate

domain where the thermal gradient is strong, thus inducing a strong vertical uplift associated with strong erosion and hydrothermal processes. Following Péron-Pinvidic *et al.* (2015), the south of the Lower Congo Basin and the Namibe Basin are associated with the upper plate domain. The Kwanza Basin is associated with a lower plate domain, but the studied wells are located close to transfer zones dividing the extending crust into segments. These zones can be either sharp (major normal crustal-scale fault) or diffuse (vague crustal and stratigraphic geometries; Péron-Pinvidic *et al.*, 2015), and infer possible complex connections between lower and upper plate domains as well as crustal fluid circulations. According to Denis and Kluska (2017), the study area is located near the Benguela Transfer zone, where the extension is highly oblique and dissects the margin in narrow stripes, offsetting structural domains apart from transverse structures, superimposing two structural fabrics.

2.2. Palaeoclimate, stratigraphy and volcanism

According to Föllmi (2012), the most important factor controlling the Early Cretaceous climates is the progressive break up of Pangaea. He established the relationships between the climate type/intensity/evolution, the tectonic and volcanic activity, the continental vegetation cover and the variations in atmospheric CO_2 partial pressure. These proxies interacted with greenhouse conditions and generated an oscillation between arid and humid conditions. Thompson *et al.* (2015) emphasized the climatic disparities along the proto-South Atlantic rift.

Presalt basins were associated with continental-lacustrine settings during syn-rift phase (Guiraud *et al.*, 2010). Pre-rift and syn-rift sediments are mainly composed of clastic and carbonate deposits reflecting continental alluvial, fluvial, and lacustrine environments (Beglinger *et al.*, 2012; Chaboureau *et al.*, 2013; Fig. 1B). The early Aptian thermal subsidence favoured the development of restricted brackish to hypersaline areas as indicated

by the deposition of coquinas, travertine and microbial carbonates on isolated platforms (Gomes *et al.*, 2009; Thompson *et al.*, 2015). The presalt carbonate and clastic deposits are overlain by widespread and massive Aptian evaporites (Karner *et al.*, 2003; Karner & Gambôa, 2007), known as the Loeme Formation in the Kwanza and Congo basins (Chaboureau *et al.*, 2013), and as the Bambata Formation in the Namibe Basin (Gindre-Chanu *et al.*, 2015, 2016). Chaboureau *et al.* (2012) concluded that those evaporitic systems were partly fed by hydrothermal recharges. A complete review of the paleogeographic and stratigraphic evolution of the presalt is available in Chaboureau *et al.* (2013).

A widespread magmatic activity occurred coevally to presalt deposits (Pereira, 1969; 1971; Marzoli *et al.*, 1999; Comin-Chiaramonti *et al.*, 2011, Teboul *et al.*, 2017). The magmatic budget changed from south to north, with magma-rich provinces in the south and magma-poor provinces in the north (Péron-Pividic *et al.*, 2015). A synthesis of the magmatic setting of the Kwanza Basin is available in Teboul *et al.* (2017). Comin-Chiaramonti *et al.* (2011) have shown that the Namibe Basin volcanic rocks follow similar trends than those from the Kwanza Basin. Gindre-Chanu *et al.* (2016) linked the volcanic rocks occurring in the Namibe Basin to the Bero Volcanics Formation, which overlie the basement. These mainly consist of tholeiitic to transitional basalts and rhyodacites interlayered with volcaniclastic and aeolian to fluvial sandstones. Likewise, the south part of the Kwanza basin registered non-negligible syn-rift and early post-rift volcanism (Aptian in age) from tholeiitic to transitional (Denis & Kluska, 2017) encountered in a number of Angola offshore wells. Little information is found in the literature on the occurrence of Cretaceous magmatism in the Congo Basin. Jackson *et al.* (2000) argue that unpublished industry seismic data indicate that volcanic rocks probably occur in this basin. Giresse (2005) reported the occurrence of kimberlitic intrusions during Cretaceous time.

2.3 Studied material

Confidentiality restrictions preclude the disclosure of the exact locations, names, and depths of the wells.

In the Lower Congo Basin, the studied samples come from two cored offshore wells (Toca-1 and Toca-2) that belong to the synrift carbonate reservoirs of the Toca Formation. This formation is intercalated between and within two source rocks, the Pointe Noire and Pointe Indienne shales (Chaboureau *et al.*, 2013). The Toca Formation (short for "top carbonate") is dominated by skeletal carbonates with a main facies characterized as "coquina" facies (Harris, 2000; Thompson *et al.*, 2015), which are presently studied from the Toca-1 and Toca-2 cored wells. This facies is characterized almost entirely by coarse (<2 cm) packstone to grainstone composed of unionid bivalves and gastropod shells, with occasional ostracod and fish remains. As stated by Thompson *et al.* (2015), coquinas were formed in freshwater to brackish lakes, at shallow depths, on horst blocks, hangingwall ramps and footwall crests of tilted fault blocks, accommodation zones, and anticlinal rollover structures.

The studied material from the Kwanza Basin (offshore Angola) has been collected on sidewall cores of the Shrubby-1 well, and from a core of the Berilo well. In Shrubby-1, part of the well has been assigned to the Cuvo Formation, composed of syn-rift fining upward litharenite/conglomerates (Bate et al., 2001). These clastic deposits are mainly overlain by dolomitic and silica-cemented carbonates and evaporites, considered as an equivalent of the Chela Formation in this study. This formation has been studied in the upper part of the well Shrubby-1 and in Berilo. The Cuvo and Chela Formations are associated with the thermal subsidence preceding salt deposition, which developed on a regional stratigraphic intra-Aptian discontinuity (San Miguel *et al.*, 2017). Carminatti *et al.* (2008) also showed that these carbonates accumulated on structural highs, which are currently located in deep-water settings offshore Angola (>1000 m below sea-level).

Two outcrops from Mariquita and Mina do Gesso (Onshore Namibe Basin, Angola) have been studied. These outcrops are respectively located 2.5 km east and 9 km north-east of the Mariquita village. Presalt deposits of the Namibe Basin are poorly described in the literature (Coterill *et al.*, 2002; Chaboureau *et al.*, 2013; Gindre-Chanu *et al.*, 2015, 2016; Schröder *et al.*, 2015). According to Gindre-Chanu *et al*. (2015, 2016), lacustrine marlstones, limestones, and microbial deposits belong to the Cangulo Formation. These microbial deposits are associated with dolomitic and siliceous bodies attributed to syn-sedimentary hydrothermal activity. The overlying formation, called by Gindre-Chanu *et al*. (2015, 2016), the "Tumbalunda Formation" consist of fluvial to alluvial fan gravelly facies, conglomeratic mouth deltaic bars, metre-thick siltstones, organic-rich mudstones, siliciclastics, evaporites, and carbonate beds formed either in lacustrine or hydrothermal setting.

3. Methods

3.1. Paragenetic sequences

Conventional optical microscopy, under plane polarized light (PPL) and cross-polarized light (XPL), was used to examine 300 polished thin sections in order to characterize microfacies and diagenetic phases such as cements, dissolution phases, fractures, and mineralogical replacements. For calcite and dolomite identification, thin sections were partially stained with alizarin red-s and potassium ferricyanide after etching in dilute hydrochloric acid (Dickson, 1966). A first order (full wave) retardation plate has been used in order to characterize the sign of elongation (length-fast or length-slow) of fibrous microquartz cements. Additional methods were applied to selected samples. These methods include the use of cathodoluminescence (referred as "CL") on a Luminoscope ELM-1 coupled with a stereomicroscope Leica MZ12 and ZEISS MRc5 camera (Burgundy University) and a CCI 8200 Mk4 coupled with a Nikon Eclipse 80i microscope and a Nikon DS-Fi1c camera

(TOTAL CSTJF RGM laboratory). UV epifluorescence microscopy was carried out on a AZ100 Nikon macroscope under a 360 nm excitation LED light. Fibrous microquartz microtextures were investigated on six rock chips using Scanning Electron Microscopy (XL30 SEM™; FEI/Philips; Université Aix-Marseille). A total of twenty-two thin sections were analysed on a Scanning Electron Microscope equipped with a Brucker Quantax EDS detector (SEM-Quantax; TOTAL CSTJF laboratory), allowing to investigate the elemental composition of specific minerals. Microthermometric measurements of fluid inclusions were carried out, when possible, using a THMS G600 Linkam semi-automatic gas-flow freezing-heating stage (Université Bourgogne-Franche Comté).

3.2. Oxygen isotopes

In situ oxygen isotope microanalysis of quartz cements was performed by secondary ion mass spectrometry (SIMS) at the CRPG in Nancy (France) using a Cameca 1280HR. Analyses of different samples were performed over six analytical sessions in two periods of three successive days (July 20^{th}-21^{st}-22^{nd}, 2015 and May 30^{th}, 31^{st}, June 1^{st}, 2016). Analyzed thin sections were finely polished (with 0.25 µm diamond), then checked for flatness and photographed using a reflected light microscope. This was done to facilitate the precise location of areas of interest (the SIMS 1280 is devoid of transmitted light visualization system) and especially to avoid areas with reliefs that are known to substantially modify measurements (Eiler et al. 1997; Valley and Kita 2009). A total of 19 thin sections from the different studied locations have been analyzed. A Cs+ beam with a 10 kV accelerating potential is used to sputters sample atoms, excavating a shallow pit in the surface (~5 µm in diameter). The ^{18}O and ^{16}O isotopes were measured on two off-axis Faraday cups, and ^{17}O isotopes on the axial electron multiplier in multicollection mode. Measurements were performed with typical counts of ~3.10^9 counts per second for ^{16}O. Acquisition sequences

consisted of 60 s of pre-sputtering and 30 cycles resulting in an internal error better than 0.1‰ ($2\sigma_n$, n = number of cycles). The external reproducibility was estimated through multiple analyses of two standards, with systematic measurements at the beginning and at the end of each session (days). The two laboratory standards (QZ-BRA and NL 615; Fouillac and Girard, 1996; Marin *et al.*, 2010) are homogenous megaquartz (Girard *et al.*, 2001) as no opal or fibrous microquartz standards are available. They are included in epoxy, finely polished, and mounted in a single cylindrical mount. For each session, the drift between first and last standard measurements was calculated, leading to an external reproducibility of $\delta^{18}O$ from ±0.1 to ±0.6 (1σ). QZ-BRA has an accepted value of 9.6±0.2‰ and NBL 615 has an accepted value of 18.4±0.2‰. Eiler *et al.* (1997) suggested that the analysis of a standard with a chemical and structural composition similar to the studied samples is needed to apply proper correction of the matrix effect (instrumental bias). Areas with epoxy-impregnated microporosity were not measured, or were not integrated in the results, in order to avoid the possible influence on this epoxy on the oxygen isotopic signal. All $\delta^{18}O$ values are expressed in permill relative to the Standard Mean Ocean Water (SMOW).

4. Results

4.1. Petrography and cement stratigraphy

The diagenetic sequences depicted in figure 2 are based on textural relationships observed in thin sections. In agreement with the scope of this study, the following paragraphs focus on the main diagenetic stages and the description of silica cements.

4.1.1. Onshore Angola

In Mariquita, the primary facies is laminated, consisting of a succession of (i) inclusion-rich radiaxial calcite layers, (ii) peloidal wackestone to grainstone and (iii) thin micritic laminae.

All these layers are intensively, but not systematically, dolomitized. When not dolomitized, the micrite is Fe-poor and non-luminescent. When dolomitized, the matrix is cryptocrystalline and has a dull to bright red luminescence. Radiaxial layers are now composed of Fe-poor and inclusion-rich dolomite, but various characteristics suggest a primary calcitic nature, as highlighted by the striking similarity with the calcitic radiaxial layers and spherulites observed in Mina do Gesso outcrops. This dolomite shows a sweeping extinction with a dull-red luminescence. Botryoids of dolomitized calcite are also observed in early fractures and form the first cements. The latter are overlain by euhedral dolomite rhombs with a dull red to brown CL and a low Fe content. Silica precipitated after a phase of fracturing and strong dissolution of calcite and dolomite (Fig. 2). In few samples, the first silica cements are isopachous or botryoidal length-fast fibrous microquartz. In most samples, silica cements are only represented by megaquartz cements (up to 1mm long) that precipitated either in primary pores, in vuggy pores, in fractures, or as a replacement of primary radiaxial calcite layers (Fig. 3A, B, C, D and E). Occasional later cements are either micritic pendant cements or Fe-poor blocky calcite with a dark red luminescence. The latter are probably of late vadose origin.

The facies studied in Mina do Gesso area are essentially composed of microbial mats displaying micritic clotted textures, with occurrences of inclusion-rich radiaxial calcite forming discontinuous layers and spherulites (Fig. 3F). Cements developed before compaction, mainly in primary fenestral porosity. The first cement is euhedral Fe-rich dolomite rhombs followed by two zones of blocky calcite displaying an orange luminescence (Fig. 2). The first one is Fe-rich and the second one is Fe-poor. Some dolomite rhombs underwent dedolomitization. Silica cements developed latter, after a phase of partial dissolution of calcite and dolomite (Fig. 2, dissolution “d1”). Most are length-fast fibrous microquartz that seals the remaining porosity (Fig. 3G). Anhedral megaquartz cements also

replace radiaxial fibrous calcite (Fig. 3F). The timing of these replacements is poorly constrained. Iron oxides, probably related to telogenesis, postdate all cements.

For both areas, an accurate quantification of quartz precipitation is particularly difficult as a sampling bias is likely influencing our observations. At outcrop scale, Mina do Gesso is poorly silicified in contrast with the extensive quartz silicification of the Mariquita section.

4.1.2. Offshore Kwanza

Two diagenetic sequences are observed in Shrubby-1 sidewall core samples and are associated with the Chela Formation and the underlying Cuvo Formation:

- The Chela Formation is composed of fibrous radiaxial calcite (*i.e.* spherulites) and shrubs-like components (Fig. 4A), which occasionally are dolomitized. Additionally, small euhedral dolomite rhombs with a dull red luminescence occur in the intergranular porosity. The shrubs, spherulites, and dolomite rhombs are enclosed in several silica cements (Fig. 2; 4A, C). From overall point of view, extensive silica precipitations occur along 93 m of the cored section, with a maximum of 95% of silicification at some stratigraphic level. The first silica cement occurs as length-slow radiaxial fibrous microquartz forming isopachous fringes and botryoids up to 500 μm thick. This cement is named porous fibrous microquartz (pfQ1) due to its frequently porous microstructure detectable both under PLL and SEM (Fig. 4 A, B, D, G, I). In PPL, the porous habit results in a blue colour due to the presence of blue epoxy resin between fibers (Fig. 4A & D). In other cases, this microporosity has been partially filled by oil, now transformed into bitumen, displaying brown patches at the periphery of pFQ1 cement (Fig. 4C). Under SEM, the fibers of pFQ1 are composed of aligned very small silica crystals exhibiting an anhedral shape and a diameter < 0.25 μm. These small crystals alternate with coarser subhedral quartz crystals (up to 3 μm long)

having their c-axis parallel to the fibers of the cement (Fig. 4G). In most thin sections, the pFQ1 cement is followed by 10 to 50 μm-thick isopachous cement characterized by alternations of equigranular microquartz and fibrous microquartz laminae (LQ1; Fig. 4). The latter is followed by a second generation of radiaxial fibrous microquartz cement with a petal like texture (referred as "petaloid") and a brown colour under PPL (pFQ2; Fig. 4D). pFQ2 was extremely microporous initially, but the microporosity between fibers is now filled with bitumen, as indicated by its brown colour (Fig. 4D). This suggests a probable syn-pFQ2 oil charge (see discussion). A new generation of 10 to 20 μm-thick isopachous laminated microquartz cement (LQ2; Fig. 4D) commonly overlaps the LQ2 petaloids. Finally, equigranular megaquartz cement (MQ), composed of euhedral colourless inclusion-poor crystals with a size up to 400 μm, fills up the remaining porosity (Fig. 4A, B, H). These successive quartz generations are considered as precompaction cements based on the evident lack of compaction features between the carbonate grains. Several fracturing stages have been observed. The first generation of fractures occurs after LQ1 and before pFQ2 precipitation. A second generation of fractures occurs before megaquartz cementation. Several fractures are also associated with microquartz cementation, but their timing is hardly constrained due to the lack of crosscutting relationships. Two successive dolomite cement phases seal a new generation of fractures associated with local calcite dissolutions: the first one shows planar euhedral crystals with dull red luminescence, whereas the second one corresponds to saddle dolomite crystals with red luminescence. These cements occur either in the remaining intergranular porosity, in fractures, or in dissolution voids located in the former shrubs. Finally, the remaining porosity is plugged by blocky calcite with a yellow luminescence, and by

bitumen. This last occurrence of bitumen is probably related to a late oil charge, based on the oil impregnations observed in the porous fibrous microquartz.

- In the Shrubby-1 well, the underlying Cuvo Formation is composed of siliciclastic deposits, basaltic beds and gabbroic bodies. The diagenetic features described below are mainly located in fractures. Firstly, the fractures are partially filled by dolomite cement, with euhedral crystals larger than 250 μm and a dull red luminescence (Fig. 2). Dolomite crystals sometimes show undulose extinction under XPL. They are enclosed in several successive generations of quartz cements starting by porous fibrous microquartz cements (pFQ) forming thick isopachous fringes or botryoids. These cements are highlighted by the blue epoxy colour under PPL. This microporosity is sometimes partially filled by oil, now transformed into bitumen. Under XPL, this cement is recognizable by its distinctive radiaxial extinction. pFQ is followed by two generations of megaquartz cements (MQ1 and MQ2) alternating with two generations of 10 to 500 μm-thick isopachous laminated microquartz cements (LQ1 and LQ2; Fig. 5A, B). As in the overlying Chela Formation, the laminated microquartz fringes are defined as alternating equigranular microquartz laminae and fibrous microquartz laminae. MQ cements shows euhedral palisadic to equigranular colourless quartz crystals larger than 400 μm in size (Fig. 5A, B). The second megaquartz cement (MQ2) is enclosed in blocky calcite cements displaying a yellow luminescence. The remaining fissural porosity contains occasional traces of bitumen.

In the Berilo well, quartz cements are observed in an intensively dolomitized facies showing ghosts of microbial laminae with fenestrae, thrombolitic micritic textures and peloidal cloths. Small subhedral dolomite crystals (< 5 μm) with an orange-red luminescence replace the initial deposits (Fig. 2). Associated euhedral dolomite crystals, < 150 μm in size, border the fenestral pores. Under PPL, this dolomite shows a cloudy

inner zone and a clean, limpid outer zone. One two-phase liquid-rich secondary fluid inclusion occurring in the outer zone provided a homogenization temperature of 109 °C. These cements are enclosed in authigenic barite, occurring as individual crystals, or combined in radiating sheaves. Many two-phase liquid-rich secondary fluid inclusions (water/gas) occurring in the barite were analyzed, yielding homogenization temperatures ranging from 50 to 120 °C. The fenestral porosity is finally totally plugged by two quartz cements i.e. botryoidal length-fast fibrous microquartz with a flamboyant texture (Fig. 5C) and a mosaic of euhedral to subhedral megaquartz crystals, ranging in size from 50 to 250 μm (Fig. 5C). Quartz cements represent around 3% of the studied facies of this well. Unfortunately, no fluid inclusions have been observed in this latter cement.

4.1.3. Lower Congo Basin

The coquina facies of the two wells studied in the Lower Congo Basin are characterized by first cements consisting of blocky calcite crystals (BC1) showing a scalenohedral habit and a succession of dull to yellow bands under CL. These calcite crystals are Fe-poor, Mg-poor and inclusion free. They developed both in interparticle and moldic pores due to an early partial dissolution of bivalve and gastropod aragonite shells. The precipitation of BC1 occurred in very shallow burial conditions, as indicated by the lack of any compaction feature. When not dissolved, the biogenic aragonite is replaced by a neogenetic inclusion-rich calcite (AC; Fig. 2) showing anhedral growth bands typical of the neogenetic replacement process. Many two-phase liquid-rich inclusions (water/gas and oil/gas) have been found and analysed in AC, indicating homogenization temperatures ranging from 70 to 180 °C and from 60 to 120°C in the Toca-1 and Toca-2 sections respectively. The secondary origin of these fluid inclusions is highlighted by their location along cleavage planes, as well as sealed microfractures. In Toca-1 samples, a second generation of blocky calcite zone (BC2; Fig. 2) took place before silica

precipitation, but after the formation of microfractures, indicating mechanical compaction. This orange to brown CL zoned cement grew syntaxially on BC1. It consists of a Fe-rich calcite as revealed by alizarine-ferricyanide staining and SEM-EDS observations. BC2 contains two phase, liquid-vapour, inclusions mainly located along cleavage planes. Microthermometric measurements in these secondary fluid inclusions provided homogenization temperatures ranging from 80 to 165 °C.

Silica cements in Toca-1 and Toca-2 precipitated after a weak dissolution of BC1 (Toca-2) and a strong dissolution of BC2 (Toca-1) cements, as revealed by dissolution vugs plugged by silica cements. Microfractures also affect shells and BC1+BC2 cements but not the silica cements. This suggests that the precipitation of silica cements occurred after mechanical compaction in the interparticle porosity (i.e. between the shells) and in the remaining moldic porosity (Fig 5D, E, F, G). In both wells, quartz precipitations are non uniform along the cored sections. In Toca-1, several silicification fronts are observed, with a maximum thickness of 10 cm, however in Toca-2, those fronts can reach 20 cm.

Successive fibrous microquartz and megaquartz cements are observed. In Toca-1 and Toca-2, the observations under PPL show a first generation of light to dark brown fibrous microquartz cement having an isopachous or a botryoidal outline. Under CL, these cements show some finely concentric laminae with alternating bluish to dark luminescence. A well-expressed sweeping extinction is detected under XPL. The use of the full wave retardation plate reveals that fibrous microquartz are length-slow in Toca-2, but length-fast in Toca-1. In the two cases, the fibrous microquartz are dense, with limited microporosity between fibers.

Megaquartz cementation mainly occurred in Toca-2, after a fracturing phase (Fig. 5F, G). These crystals display a sweeping extinction under XPL and alignments of solid inclusions

displaying chevron structures along growth bands. Neither biphasic liquid/gas inclusions nor oil-rich inclusions have been detected in these megaquartz crystals.

A single phase of blocky calcite postdating silica cementation is observed in Toca-1. This Fe-rich, blocky calcite has an orange colour under CL. In Toca-2, the diagenesis postdating silica cements is more complex and is composed of one generation of dolomite and two generations of blocky calcite. The dolomite rhombs are euhedral, Fe-poor, and exhibit three successive red to dark red zones under CL. In Toca-1 and Toca-2 the late cements consist of Fe-rich blocky calcite zones with a dark orange to brown luminescence. These late blocky calcites locally precipitated in fractures that crosscut silica cements. The remaining porosity is locally filled with bitumen.

4.2. Oxygen isotopes

The $\delta^{18}O$ values measured by SIMS in the silica cements at the different studied sites are compiled in Figure 6 and are reported in a supplementary data file that contain both data and extra microphotographs (#supplementary data 1). A total of 203 values are measured, showing an extremely large range going from ~20‰ to ~40‰ and covering about 50% of the documented range of $\delta^{18}O$ variation in rocks & minerals of sedimentary origin (i.e. 0-40‰). The microporous length-slow fibrous microquartz cements tend to show elevated $\delta^{18}O$ values, ranging from 33 to 37‰ in Shrubby-1 (33 to 35‰ (N=4) in the Chela Formation and 33 to 37‰ (N=4) in the Cuvo Formation) and 31 to 32‰ (N=9) in Toca-2. The non-porous length-fast fibrous microquartz cements tend to show somewhat lower $\delta^{18}O$ values, ranging from 28 to 31‰ (N=10) in Berilo, 29 to 32‰ (N=25) in Toca-1 and around 28‰ (N=4) in Mina do Gesso.

The laminated microquartz in Toca-2 shows very variable $\delta^{18}O$ values ranging from 27 to 33‰ (N=30). This is also true of the laminated microquartz in Shrubby-1, where $\delta^{18}O$ values range from 27 and 30‰ in the Chela (N=2) and 32 to 39‰ (N=8) in the Cuvo Formation.

The greatest overall variability in $\delta^{18}O$ values is observed in the megaquartz cements (Fig. 6), although values can be pretty consistent in a single site. $\delta^{18}O$ values range from 21 to 30‰ (N=38) in Mariquita, 30 to 34‰ (N=16) in Toca-2, 29 to 30‰ (N=5) in Berilo, and 20 to 40‰ in Shrubby-1 (33 to 40‰ (N=23) in the Chela Fm. and 20 to 38‰ (N=25) in the Cuvo Fm.) The highest $\delta^{18}O$ values of 39-40‰ measured in this study come from the megaquartz in the Chela Formation and are amongst the highest values ever reported for quartz. The lowest $\delta^{18}O$ values of 20-21‰ recorded in our dataset come from the latest growth stage of the megaquartz cement (Fig. 5B) in the Cuvo Formation. When possible, the small analytic spots (10–20 microns in diameter) were situated along transects in order to document any spatial-temporal variability in the $\delta^{18}O$ values of single cement (Fig. 3E, G; 5B, C, E). The only observed trend occurs in a Mariquita sample showing a $\delta^{18}O$ increase through time by a few ‰ (Fig. 3E).

5. Interpretation and discussion

5.1. Source of aqueous silica during presalt diagenesis

As stated by Hesse (1988, 1989), silicification is a common diagenetic process occurring in non-siliceous sediments. Several authors discussed the silica budget in oceanic (e.g. Heath, 1974; Riech & v. Rad, 1979; DeMaster, 1981; Hesse, 1988; Tréguet *et al.*, 1995) and continental (e.g. Cornwell & Banahan, 1992; Arai & Fukushima, 2012; Pittari *et al.*, 2016) settings. According to DeMaster (1981), some of the major sources of dissolved silica in marine waters are: (1) rivers, (2) active volcanism and associated hydrothermal emanations, (3) epigean weathering of volcanic rocks, and (4) dissolution of siliceous biogenic tests in

sediments. In lacustrine sediments, similar silica sources have been documented (Livingstone 1963; Renaut *et al.*, 1998; Alexandre *et al.*, 2004), but Bustillo & Alonso-Zarza (2007) also emphasized the possible contribution of the dissolution or alteration of clay minerals.

In Presalt rocks, dissolution of siliceous biogenic tests is not considered as a possible source of silica during diagenesis because marine organisms forming opal-A tests (radiolarians, siliceous sponges, silicoflagellates…) have never been observed in the continental to paralic sediments of the studied sites. Diatoms are also absent in the Presalt lacustrine sediments of the studied area.

A very likely source of dissolved silica in Presalt diagenetic fluids is the alteration of volcanic products (Tosca & Wright, 2015; Szatmari & Milani, 2016; Teboul *et al.*, 2017). This alteration could have taken place either in catchment areas, in lakes, or in the substratum beneath the lakes through hydrothermal processes. A similar source of Si has been suggested for the continental rift basin of Limagne (Massif Central, France) where length-slow fibrous silica developed within lacustrine carbonate formations, in close association with brecciated volcanic material and bitumen (Devouard & Bornet, 2015). Cerling (1994) showed that the drainage of volcanics in surrounding catchments has a strong influence on the chemistry of the lakes of the African Rift Valley. It tends to highly increase alkalinity, producing dilute waters which chemical composition is dominated by calcium, magnesium, and silica. Furthermore, interaction of saline waters would be poor in alkaline earths (Cerling, 1994). In addition, the occurrence of syn- to post-sedimentary volcanism associated with hypogean to epigean springs feeding the lacustrine systems, may have induced high CO_2 input, high alkalinity, and high concentrations of dissolved silica, magnesium, and calcium (Wright, 2012; Teboul *et al.*, 2017). Numerical modeling shows that the hydrothermal and meteoric alteration at variable temperature and CO_2 partial pressure of trachytes from a buried presalt

sequence favors high Si and Mg concentrations (Teboul *et al.*, 2017). Presalt volcanism is characterized by bimodal, mafic and felsic, rocks including silica-saturated basalts and rhyolitic end members (Marzoli *et al.*, 1999). Based on the abundance of calcite and Mg-silicates and on the absence of chlorides and sulphates, several authors highlighted that the weathering of basic volcanic formations are probably the main source of elements in presalt systems (Tosca & Wright, 2015; Szatmari & Milani, 2016). However, geochemical simulations designed to evaluate the exact contribution of the presalt basaltic volcanism to the diagenesis of Presalt deposits are yet to be conducted.

Several authors also described the influence of chemical weathering of volcanic debris and lavas in lacustrine systems as a source of solutes (e.g. Abdelouas, 1996; Garcia-Romero *et al.*, 2005). The alteration products of glass-rich volcanic ash tend to produce Si-rich gels, Fe-rich oxy-hydroxides, clay minerals and zeolites (Abdelouas, 1996). Such alterations may have a direct impact on lake chemistry through the dissolution of volcanic glass, or an indirect impact through precipitation of "intermediary media" such as clays/zeolites. According to Millot (1970) in Tosca & Wright (2015), in close basin settings associated with alkaline fluids, Al- to Fe-rich clay minerals are located along the basin margins, where aluminosilicate detritus are abundant, while Mg- and Si-rich (and Al-poor) clay minerals are located in the center. Mg- and Si-rich clay minerals are common in presalt deposits on the Brazilian margin of the South Atlantic Ocean, in particular the phyllosilicate stevensite ($Na_{0.3}Mg_{2.7}Si_4O_{10}[OH]_2$; Thompson *et al.*, 2015; Tosca & Wright, 2014; 2015; Wright & Barnett, 2015, Goldberg *et al.*, 2017). Precipitation of Mg-silicates is favored at high pH (≥8.7) and Mg/Si ratio (≥0.67) in saline waters (Tosca and Wright, 2014; 2015; Zeyen *et al.*, 2015). If altered, clay minerals could represent an important source of silica during diagenesis (MacKenzie et al., 1967; Thiry & Maréchal, 2001; Michalopoulos & Aller, 1995, 2004). Several authors emphasized that early to late diagenetic alteration of Mg-silicates

controlled, among other things, by pH or CO_2 partial pressure fluctuations, would result in the release of Mg, Si, and minor Na (eg. Deocampo, 2005; Tosca & Wright, 2014; 2015). This alteration may have contributed to dolomitization and silicification processes in presalt deposits.

The actualistic comparison with published data reveals that many of the modern silica-rich waters are related to rift settings, and more particularly to lakes and springs of the East African Rift System (Eugster & Jones, 1968; Dunkley *et al.*, 1993; Sturchio *et al.*, 1993; Behr & Röhricht, 2000; Renaut *et al.*, 1998, 1999, 2002; Dekov *et al.*, 2014). Other case studies are usually associated with volcanic geological setting such as Specchio di Venere (Italy; Cangemi *et al.*, 2010), Mono Lake (USA; Souza-Egipsy *et al.*, 2005), Cachi Laguna and Pastos Grandes (Bolivia; Risacher, 1978; Abdelouas, 1996; Sylvestre *et al.*, 2001), and Azores Islands (Brunet & Bustillo, 2014). Several authors attributed the occurrence of these silica-rich waters to the prevalence of closed-basin conditions and the primary inflow of alkaline sodium carbonate/bicarbonate springs associated with volcanic material (Kempe & Degens, 1985; Abdelouas *et al.*, 1995; Abdelouas, 1996; Garcia-Ruiz, 2000). This agrees with the hypothesis advocated for presalt environments, stating that silica-rich fluids are derived from altered volcanic material. However, modern environments are often associated with diatom frustules. We consider that these frustules may act as silica-rich intermediary media, as the biomineralized silica is probably derived from the alteration of catchment areas.

Following the work of Ambwani *et al.* (2003), the studied Early Cretaceous rocks are probably too old to use diatoms as intermediary silica source. In the modern deposits of Cachi Laguna (Bolivia), Abdelouas (1996) evidenced a close relationship between the occurrence of silhydrite (an hydrated form of silica: $3SiO_2[H_20]$), magadiite (hydrated sodium silicate) and stevensite-saponite, associated with the dissolution of nearby silicates,

rhyolitic volcanic glass, and diatom frustules. The latter author attributed the direct precipitation of silhydrite to low Na concentrations of hydrothermal waters, whereas magadiite tends to precipitate in Na-rich waters in the central part of the lake. Stevensite precipitation would be favored through the dissolution of the diatom frustules, in Mg-rich, alkaline setting, where silanol groups are available for clay precipitation. The Cachi Laguna area may therefore constitute a great location to establish the spatial and temporal relationships between volcanic material alteration, Mg-rich clay minerals and silica precipitation. In this case study, the potential of hydrated silica deposits to be remobilized or neomorphized during diagenesis should be investigated.

Finally, a recent study conducted by Pinto *et al.* (2016) evidenced that serpentinization of mantle rocks may also constitute a source of silica. These authors established mass balance calculations based on material from exhumed and serpentinized domains from Western Iberia and fossil Alpine Tethys margins. By extrapolation, they suggested that similar elemental transfers can occur in nascent oceanic basins, prior to seafloor spreading. Following the recent geodynamic models implying upper and lower plate domains, the exhumed mantle could have been coupled to presalt sediments through lithospheric-scale low angle detachment faults, enabling large-scale fluid circulation that may have influenced the presalt sedimentary-diagenetic evolution (Unternehr *et al.*, 2010; Péron-Pinvidic *et al.*, 2015).

In this study, the spatial distribution of quartz precipitation between the different sites is non uniform. The most extensive precipitations have been observed in the well Shrubby-1 and in the onshore outcrop of Mariquita. The vertical and lateral variation of silica content is probably related to differential amounts of silica supply during diagenesis of each studied area. Following the available knowledge of the presalt series, we consider that the most

probable sources of silica may be associated with the alteration of volcanic material or with fluids linked to mantle rock serpentinization.

5.2. Timing between carbonates and silica cementation

Some carbonate diagenesis predates silicification at all studied sites (Fig. 2). The earliest diagenetic processes include carbonate cementation and neomorphism, and are highlighted by: (i) a strong dolomitization and/or euhedral dolomite precipitation filling pores (Mariquita, Shrubby-1, Mina do Gesso, Berilo), and (ii) aragonite to calcite neomorphism of shells and blocky calcite cementations (Toca-1 and Toca-2). An early diagenesis controlled by carbonate precipitation is particularly consistent with presalt carbonate dominated sedimentary systems (Terra *et al.*, 2010; Gindre-Chanu *et al.*, 2016; Saller *et al.*, 2016). Typical presalt carbonates are composed of shrubby microbial boundstone, and wackestone to packstone bearing calcitic spherulites in a dolomitic to argillaceous matrix (Terra *et al.*, 2010; Saller *et al.*, 2016; Goldberg *et al.*, 2017). Such primary calcite (Mariquita and Mina do Gesso) and eventual primary dolomite (Berilo) structures are indeed observed in our studied material. This implies that a sedimentary-diagenetic continuum existed between the carbonate-rich lacustrine to paralic system and early diagenetic processes. The nature and succession of early diagenetic features support a continuum through precompaction cementation, the spherulites, and the cemented coquina. The fact that diagenetic silica comes later in the diagenetic succession, after a significant phase of calcite-dolomite diagenesis, constitutes an argument against the occurrence of sinter-like subaerial deposits at our studied sites, as silica would have represented the primary sedimentological and early diagenetic products. However, this observation does not preclude a relatively early formation of silica cements in the Mariquita outcrops and in the Chela Fm in the Shrubby-1 well, as in these two sites, silica cements precipitated before any significant mechanical compaction. This pre-

compaction diagenesis is exceptional in Mariquita, where the texture of primary carbonate deposits is particularly well preserved. Saller *et al*. (2016) also reported early pre-compaction silicification in the offshore Kwanza Basin, based on occurrence of intraclasts with truncated chalcedony cements interpreted as silica precipitation during spring mound-like deposition. This indicates that silica diagenesis started at the sediment/water interface or within shallow burial settings. In other studied sites, silicification may have occurred at a later time. In Mina do Gesso and Berilo, silica cement occurs in residual pore spaces that have survived a significant carbonate/sulfate cementation phase, suggesting silica precipitation took place during later diagenetic stages. Based on petrographic observations, quartz precipitation postdates the formation of microfractures which affect only shells and predates blocky calcite cementation in Toca-1 and Toca-2 studied sites. This suggests that quartz cementation occurred after the first steps of mechanical compaction. Finally, the silica cements of the Cuvo Fm. in the Shrubby-1 well occur mainly as fracture filling, cross-cutting moderately to strongly indurated sandstones and exhibiting fluid inclusions with homogenization temperatures around ~100°C, thereby possibly suggesting a possibly advanced burial stage or an abnormal geothermal gradient linked to volcanic activity (Girard & San Miguel, 2017; Girard et al. 2017).

5.3. Insights from the partition between length-slow and length-fast fibrous microquartz

Petrographic and geochemical investigations of the quartz cements highlights a bimodal partitioning amongst the different studied sites, based on: (1) the length-fast vs. the length-slow habit of the fibrous microquartz, (2) the greater carbonate dissolutions associated (prior) to length-fast fibrous microquartz precipitation, and (3) the increase in $\delta^{18}O_{quartz}$ values from length-fast to length-slow fibrous microquartz. We suggest that this textural and geochemical

partition between the two fibrous microquartz habit may be an indicator of the environmental conditions of precipitation. Originally, Folk & Pittman (1971) described these quartz habit. Warren (2016) reviewed and discussed the latter in light of their precipitation processes. Length-fast cements would be associated with neutral to acidic environments because high Si concentrations and low pH favor the polymerization of monosilicic acid ($Si(OH)_4$) groups. Such groups would likely precipitate tangentially on the precipitation surface (Folk & Pittman, 1971). In contrast, high pH tends to favor the occurrence of monomeric $Si(OH)_4$ tetrahedra, inducing that length-slow fibrous microquartz reflect alkaline environments. The chemical behavior of silica in function of pH is explained by Iler (1971). Arbey (1980) discussed extensively Folk & Pittman's (1971) observations and pointed out the potential control of dissolved sulphates on quartz precipitation. Sulphate-rich environments would favor the precipitation of length-slow fibrous microquartz cements, whereas sulphate-poor environments would favor length-fast forms. Unfortunately, petrographic or geochemical evidence for a former presence of sulphates in the studied samples is lacking. Bustillo *et al.* (2012) reported similar observations as Folk & Pittman (1971) in the Miocene continental cherts from the Madrid Basin (Spain), and linked the occurrence of length-fast fibrous forms to carbonate sedimentary settings lacking dolomite or gypsum. Conversely, they related the precipitation of length-slow fibrous forms to Mg-rich palustrine evaporitic environments associated with gypsum, dolomite, and Mg-clay minerals. As explained previously, the most probable Si source leading to quartz precipitation in the presalt series is alteration of volcanic rocks, with a possible contribution of mantle rocks through hydrothermal activity. Deep hydrothermal contribution in rift settings linked to the mantle has reported by Lee et al. (2016). The alkalinity, pH, and elemental concentrations of the presalt diagenetic fluids may have been strongly controlled by the nature of rocks prevailing in the palaeohydrological catchment/basin (e.g. Teboul *et al.*, 2017). Teboul *et al.* (2016) documented such a process in

recent and modern continental carbonate settings: fluid/rock interactions involving mantle rocks in the Voltri massif of the Ligurian ophiolites (Italy) lead to highly alkaline fluids, in agreement with other observations on Oman Ophiolites (Chavagnac *et al.*, 2013; Leleu *et al.*, 2016). Similarly, it has been demonstrated that fluid/rock interactions of basic volcanic rocks of Reunion Island (Indian Ocean) lead to neutral to alkaline fluids (Teboul *et al.*, 2016). The alteration of presalt acid volcanic rocks in the offshore Kwanza basin (Angola) would have led to near neutral to slightly acid fluids, depending on the amount of CO_2 during fluid/rock interaction (Teboul *et al.*, 2017). Deocampo & Renaut (2016) emphasized such interaction in the soda lake of the east African rift. As shown by several authors (Pereira, 1969; 1971; Marzoli *et al.*, 1999; Comin-Chiaramonti *et al.*, 2011), the early Cretaceous volcanic rocks from Angola include a wide spectrum of compositions, from basalts to rhyolites, while that of late Cretaceous volcanic rocks ranges from basalts to trachytes. In light of these results, we assume that variable water chemistry and pH could have occurred in presalt palaeohydrological basins, reflecting the heterogeneity of presalt basement and strata, and structural heritage. We therefore postulate two major end members. The first implies ultramafic/basic volcanic rocks, which can lead, through fluid/rock interaction, to the production of Si-rich alkaline diagenetic fluids. Such fluids would be prone to form length-slow fibrous microquartz. The second end member results from interactions with intermediate/acid volcanic rocks, producing Si-rich neutral to acidic diagenetic fluids, prone to form length-fast fibrous microquartz. The occurrence of significant dissolution features observed prior to silica cementation supports the hypothesis of an acidic diagenetic fluid associated with length-fast fibrous microquartz, in Mina do Gesso, Mariquita, and Toca-1 studied sites.

From a thermodynamic point of view, the solubility of silica polymorphs is significantly greater in strongly basic pH conditions (e.g. greater than 9 at 25°C or greater than 8 at 100°C;

Fig. 7; Iler, 1979). This implies that under basic conditions supersaturation will be reached only at extremely high dissolved silica concentrations. Fig. 7 also illustrates that temperature plays a prominent role in the precipitation of silica polymorphs. It can be seen that the solubility of silica polymorphs is about one order of magnitude greater at 100°C compared to 25°C. Consequently, high temperature waters are prone to carry high dissolved silica content and any decrease in fluid temperature would induce silica precipitation, either as fibrous microquartz or quartz depending on the initial dissolved silica concentration (Fig. 7).

The microporous fabric of the length-slow fibrous microquartz observed in Shrubby-1 is a peculiar texture/feature. To our knowledge, only a few authors described similar cements in deeply buried carbonate sequences, e.g. Saller *et al.* (2016) in the Kwanza basin (Angola) and Watney & Rush (2012) in the Arbuckle Group saline aquifer (Kansas, USA). In the present study, observations indicate that the porous fibrous microquartz shows a strong interrelationship with oil, suggesting that oil emplacement may have started coevally or shortly after fibrous microquartz precipitation. The decomposition of organic matter may also favor early silica precipitation as increasing CO_2 partial pressure, through oxidation of organic matter, leads to a simultaneous increase of carbonate solubility and decrease of silica solubility (Gao & Land, 1991; Smrzka *et al.*, 2015). It is commonly accepted that fibrous microquartz probably indicates extremely high precipitation rate in highly supersaturated fluids (García-Ruiz, 2000; Warren, 2016). The migration of hydrocarbons soon after precipitation of microquartz fibers may have inhibited further development of quartz overgrowths on the fibrous microquartz, thus preserving its microporosity. An early oil migration in a rift setting can result from the prevalence of elevated thermal regimes, possibly associated to volcanic activity (Ziegler, 1992; Pindell, 1995; Chen *et al.*, 1999). The Limagne Basin (Massif Central, France) represents a valuable analog of a continental rift system showing the relationship between magmatic activity, carbonate precipitation, oil migration,

and siliceous cementation in shallow buried lacustrine sediments (Wattinne, 2004; Couturié, 2015).

It has been noticed above that high $\delta^{18}O_{quartz}$ occurs in porous length-slow microquartz cements in Toca-2 and Shrubby-1 compared to the length-fast non-porous microquartz found in Toca-1, Berilo and Mina do Gesso (Fig. 6). In former studies, $\delta^{18}O_{quartz}$ measurements on siliceous cements have mainly been carried out on cements formed from seawater in Precambrian-Phanerozoic marine sediments with the aim of investigating their temperature of formation (Knauth & Lowe, 1978; Marin-Carbonne *et al.*, 2014; Knauth & Epstein, 1976). In such studies, reconstructing the temperature of formation of the silica cement based on its $\delta^{18}O_{quartz}$ signature is possible because they formed from seawater of which the oxygen isotope composition can be constrained. Such an approach cannot be used for the early silica cements of the presalt deposits, because the parent water is thought to be of continental origin and its oxygen isotope value is unknown. Microthermometry measurements of primary fluid inclusions in the silica cement could help constraining their formation temperature. However, the presence of fluid inclusions is impossible to ascertain due to the fibrous nature of the cement. Nevertheless, indirect temperature and isotopic constraints can be derived from the published information. According to palaeoenvironmental reconstructions proposed by Chaboureau *et al.* (2013), the studied area was located in the tropical zone during Aptian time (Fig. 1B). This suggests that lake water temperature was unlikely to be much below ca. 25°C. Accordingly, we used this value as a minimum temperature of crystallization for early fibrous microquartz cements in Fig. 8A ("T"). According to Shackleton & Kennett (1975) and Sheppard (1986), the mean isotopic composition of the ocean before the Miocene was about $\delta^{18}O_{water}$= -1‰. However, Veizer et al. (1986) showed that the seawater composition was not uniform through time. Although, the same author showed that the major variation occurs in the Early and Mid-Paleozoic oceans. Considering that the $\delta^{18}O_{water}$ of Aptian sea water was

on the order of -1‰, all $\delta^{18}O_{water}$ values below -1‰ can be interpreted as tracing a meteoric influence, and values greater than 0‰ can be attributed to magmatic, evaporated or highly modified waters (Criss, 1999; Hoefs, 2009). Magmatic waters are defined by Criss (1999) as waters of any origin that has equilibrated with magma. Following Sheppard (1986), the $\delta^{18}O_{water}$ values of "primary magmatic water" can reach approximately 10‰, following equilibrium with crystalline rocks at igneous temperatures. Similar isotopic composition would be expected in a volcanic setting where deep hypogean fluids are exposed to igneous temperatures (Sheppard, 1986; Taran et al, 1995). These waters differ from hydrothermal waters, which are predominantly derived from local meteoric waters (Craig et al., 1956), and can show elevated $\delta^{18}O_{water}$ values (up to 20 ‰ or more) as a result of water/rock interactions with ^{18}O-enriched rocks. Of course, evaporation processes can also produce significantly ^{18}O-enriched waters (up to 10‰). High to extremely high $\delta^{18}O_{water}$ values have been reported in evaporative settings, i.e. 11.3‰ in Lake Baringo, Kenya (Renaut *et al.,* 2002) or 31.3‰ in small, shallow lakes of the Western Sahara (Gonfiantini, 1986), but such values remain exceptional. Boiling can also enhance $^{18}O_{water}$-enrichment (Bottinga & Craig, 1969). This shows that during boiling, ^{18}O partitioning into the liquid phase can lead to strongly enriched $^{18}O_{water}$. The above information and constraints provide an interpretative frame for our results, which are further discussed below.

The large spread in $\delta\ ^{18}O_{quartz}$ data reported in this study is noteworthy (Fig. 6). This heterogeneity of isotopic values can reflect temperature variations or changes in fluid composition at microsite scale. Processes other than temperature and initial parent $\delta^{18}O_{water}$ may affect the $\delta^{18}O$ of quartz/silica; including growth under disequilibrium conditions (Dickson, 1991), sector zoning (Jourdan et al., 2009), variable incorporation of trace Al in the quartz lattice due to a change from normal step-wise growth to spiral growth (Yoshimura et al., 1979; Larkin et al., 1982). In fibrous microquartz cements, minor $\delta^{18}O$ variations could

also be related to the occurrence of OH-related impurities. In general, fibrous microquartz cements tend to contain approximately 2 wt.% of silanol (SiOH) and water (H_2O), with water located mainly in very small fluid inclusions (Flörke *et al.*, 1982; Schmidt *et al.*, 2013). The strong variation of $\delta^{18}O$ values observed by using SIMS analysis highlight the necessity to be careful of bulk quartz and chert $\delta^{18}O$ as it can homogenize true values of multiple quartz generations. Similar observations have been shown in several recent studies (Denny *et* al., 2017; Cammack *et al.*, 2018). However, the possible influence of the processes listed previously in the large $\delta^{18}O$ values spread observed in this study cannot be assessed at this time. As a consequence, it will not be discussed further.

Despite the difficulty to use $\delta^{18}O_{quartz}$ as a geothermometer, the elevated $\delta^{18}O_{quartz}$ values measured in the Presalt cements provide valuable information. Saller *et al.* (2016) suggested that such elevated values reflect an evaporitic source of the quartz-forming waters in the presalt sediments. In our study, the oxygen isotopic compositions of water have been extrapolated to low temperatures based on the fractionation factor of Matsuhisa *et al.* (1979) for the quartz-water system. We consider that there is no significant differences between this fractionation factor and the calibrations of Clayton *et al.* (1972) or Hu & Clayton (2003). The length-slow porous microquartz cements show a maximum value of 37‰ (Fig. 6). Considering the minimum temperature of T=25°C, the $\delta^{18}O_{water}$ values would be of at least 0‰ (Fig. 8A) and possibly higher if a higher temperature of formation is considered, i.e. 15‰ at a temperature of 100 °C (Fig. 8A) which would represent extreme conditions of water evaporation. High $\delta^{18}O_{quartz}$ (44‰) were also obtained from microquartz precipitating in evaporative environments from the East African Rift (Fig. 9; O'Neil & Hay, 1973). Literature data of quartz precipitated during early to late marine diagenesis exhibit $\delta^{18}O_{quartz}$ values consistent with the global range compiled in this study (Fig. 9). In the past, several authors interpreted high isotopic values as the expression of very low temperature of

crystallization (usually <5 °C), consistent with deep oceans conditions (Degens & Epstein, 1962; Knauth & Epstein, 1975). As indicated above, such low temperatures are incompatible with the presalt depositional environments. As shown in Fig. 9, the range of $\delta^{18}O_{quartz}$ values (20-40‰) measured in the Presalt silica cements has never been documented in any other non-evaporitic sedimentological or diagenetic setting.

The length-fast and length-slow non-porous microquartz cements exhibit statistically lower $\delta^{18}O$ values (27-32‰) than their length-slow porous counterpart (33-37 ‰). The lowest value for length-fast fibrous microquartz in Toca-2 is 27‰, which implies that the $\delta^{18}O_{water}$ would have been lower than 0‰ (i.e. meteoric or mixed meteoric-marine) at all temperatures below 60 °C (Fig. 8A). For the megaquartz cements, the highest $\delta^{18}O_{quartz}$ of 40‰ was measured in Shrubby-1 (Fig. 6). Saller *et al*. (2016) reported a similar maximum $\delta^{18}O_{quartz}$ value of 41‰ in the presalt megaquartz cements in offshore Kwanza (Fig. 9). Girard & San Miguel (2017) and Girard et al. (2017) reported primary two-phase fluid inclusions in megaquartz cement in the Presalt carbonates of an offshore Kwanza well yielding homogenization temperatures clustering around ~100°C. The latter authors also emphasized that the presalt deposits at that location were submitted to elevated temperatures, approaching ~200°C. Poros *et al.* (2017) documented homogenization temperatures ranging from 98 to 123°C for fluid inclusions occurring in chalcedony and megaquartz cements in the Omosi-1 well, offshore Kwanza. Based on this information we can constrain the temperature of crystallization of the megaquartz cement in our samples to be between 100 and 200°C (Fig. 8B, "T2" and "T3"). At such temperature, the measured $\delta^{18}O_{quartz}$ values would mainly reflect precipitation from highly ^{18}O-enriched waters. Only the two lowest $\delta^{18}O_{quartz}$ values in our dataset would be compatible with a modified marine water signature (Fig. 8B). Girard et al. (2017) favor the influence of pervasive hydrothermal waters based, among other things, on the omnipresence

of highly saline fluid inclusions (>200 g/l) in the successive cements (dolomite, calcite, quartz) found in the studied samples of the presalt carbonates.

5.4. Proxies controlling silica precipitation: scenarios

Following the elements discussed above, we propose that the different habit and geochemistry of the different quartz cements were probably controlled due to fluid/rock interaction with two substratum end-members (respectively intermediate to acid substratum and basic to ultramafic substratum). From basin to pore scale, four main steps from early to late burial diagenesis can then be described as follows (Fig. 10):

- Step 1: at basin scale, at several sites (Mariquita, Berilo, Toca-1, Mina do Gesso), ^{18}O-depleted fresh to slightly evaporated waters could have interacted with intermediate to acid volcanic substrates, promoting circulation of Si-rich neutral to acid waters in the sediment (Fig. 10-1A). At other sites (Shrubby-1, Toca-2), hypogean fluid/rock interaction between ^{18}O-enriched slightly to highly evaporated water and basic to ultramafic basement would promote intra-sedimentary circulation of Si-rich alkaline waters (Fig. 10-1B). In both case, the initial fluid isotopic composition could have been undifferentiated if we consider that the final ^{18}O composition of the water is only influenced by water/rock interaction along the hydrogeological pathway.
- Step 2: at pore scale, after precipitation of carbonate cements close to the sediment/water interface, circulation of Si-rich waters during early diagenesis induced partial carbonate dissolution, especially when Si-rich acidic waters interacted with the sedimentary body (Fig. 10-2A).
- Step 3: in agreement with Folk & Pittman (1971), the intense circulation of neutral to acidic waters, very rich in $Si(OH)_4$ polymers (due to acidic pH), promoted rapid

precipitation of length-fast fibrous microquartz displaying the lowest $\delta^{18}O_{quartz}$ values (Fig. 10-2A to 3A). Conversely, the intense circulation of alkaline waters very rich in ionized $Si(OH)_4$ tetrahedra promoted rapid precipitation of length-slow fibrous microquartz characterized by the highest $\delta^{18}O_{quartz}$ values (Fig. 10-2B to 3B). In case of early oil impregnation, the length-slow fibrous microquartz cement may have preserved microporosity between individual fibers during later diagenetic processes (Fig. 10-3B').

- Step 4: at most sites, the silica diagenesis ended with megaquartz precipitation during early to burial diagenesis, usually associated with hydrothermal circulations (Girard & San Miguel, 2017; Girard et al., 2017; Poros *et al.*, 2017) possibly driven by geothermal convection below the salt cover (Jones & Xiao, 2013). Highly ^{18}O-rich megaquartz cementations followed the precipitation of length-slow fibrous microquartz (Fig. 10-4B), in accordance with the interaction of strongly enriched waters along this diagenetic pathway. Further work is needed to better constrain the conditions of precipitation of the late quartz cements.

6. Synthesis and conclusions

The integrated petrographic and geochemical study of quartz cements occurring in the presalt rocks from offshore and onshore basins of the West African margin provides valuable information to constrain the palaeoenvironmental and diagenetic settings. This study is the first attempt to combine $\delta^{18}O_{quartz}$ values with the length-fast vs. length-slow habit of fibrous microquartz cements. Several potentially useful markers are highlighted by the study and are summarized below:

- Early length-slow fibrous microquartz cements precipitated from Si-rich, alkaline waters. $\delta^{18}O_{quartz}$ values range from 31 to 37‰, reflecting formation from evaporated

water at probably low temperature (<100°C). The required alkaline nature of these waters is probably linked to fluid/rock interactions involving basic volcanic rocks, with a possible mantle influence. A mantel influence would be particularly consistent with the recent geodynamic models established for the South Atlantic margins. Early to late length-fast fibrous microquartz cements with $\delta^{18}O_{quartz}$ values ranging from 27 to 32‰, precipitated from moderately to non-evaporated water at higher temperatures. Influence of marine water cannot be excluded if temperature was between 35 and 60°C. The length-fast cements require Si-rich neutral to acidic waters, probably derived from interaction with intermediate to acid volcanic rocks. Such interactions are consistent with field and well data, documenting the existence of magmatic intrusions and hydrothermal alteration. The characterization of length-fast vs. length-slow habit of fibrous microquartz holds great potential to unravel the paleo pH history of the parent waters.

- A peculiar form of length-slow fibrous microquartz cements is described which shows abundant preserved interfibre porosity often impregnated by oil. Such cements have not been investigated in the literature and would certainly deserve more attention in order to unravel the link between early oil migration and early quartz precipitation in alkaline, saline waters.
- Megaquartz following length-slow fibrous microquartz exhibits $\delta^{18}O_{quartz}$ values up to 40‰, that are indicative of highly ^{18}O-rich waters, most likely including a significant contribution of recycled evaporated waters or strong water/rock interaction. Strong variations in $\delta^{18}O_{quartz}$ values can reflect temperature variations or changes in fluid composition. This would indicate a strong heterogeneity of thermo-chemical conditions at microsite scale. Megaquartz is likely associated with lower cementation

rate and dissolved silica concentration in the diagenetic waters compared to fibrous microquartz.

In order to further investigate and understand the conditions of quartz cementations in the studied Presalt deposits from the South Atlantic more detailed fluid inclusion work should be conducted. Such an approach should also be applied to the onshore and offshore Presalt basins of the Brazilian margin, in order to reconstruct a global and possibly predictive model of quartz cementation in Presalt series. Moreover, several authors have highlighted that dissolved sulphates may also control the habit of quartz during precipitation. Unfortunately, no information on the occurrence of former sulphate-rich minerals was recorded in the studied intervals.

Acknowledgments

We acknowledge TOTAL E&P for funding the project and for granting permission to publish. Thanks are expressed to Nordine Bouden, Michel Champenois and Etienne Deloule from the CRPG-CNRS for the access to the SIMS and for their precious analytical help. We would like to warmly thank Anneleen Foubert and David Jaramillo-Vogel for the discussions and early work on the samples from the Namibe Basin, as part of their collaboration with Total E&P. Thanks to Eric Verrecchia, Jacques Pironon, Catherine Lerouge, and Bruno Hamelin for the precious discussions about this work.

References

Abruzzese, M.J., Waldbauer, J.R., Chamberlain, C.P., 2005. Oxygen and hydrogen isotope ratios in freschwater chert as indicators of ancient climate and hydrologic regime. Geochimica et Cosmochimica Acta, 69(6), 1377-1390.

Abdelouas, A., 1996. Etude de l'altération de verres rhyolitiques au contact de saumures naturelles (Bolivie) — Application à l'étude du comportement à long terme du verre nucléaire R7T7. PhD thesis, Institut für Nukleare Entsorgungstechnik, 245 pp.

Abdelouas, A., Crovisier, J.L, Lutze, W., Ullman, W.J., Risacher, F., 1995. Occurrence of silhydrite in a soda lake on the Bolivian altiplano. Clay Minerals, 30, 77–82.

Alexandre, A., Meunier, J.D., Llorens, E., Hill, S.M., Savin, S.M., 2004. Methodological improvements for investigating silcrete formation: petrography, FT-IR and oxygen isotope ratio of silcrete quartz cement, Lake Eyre Basin (Australia). Chemical Geology, 211, 261–274.

Alonso-Zarza, A.M., Genise, J.F., Verde, M., 2011. Sedimentology, diagenesis and ichnology of Cretaceous and Palaeogene calcretes and palustrine carbonates from Uruguay. Sedimentary Geology, 236 (1–2), 45–61.

Ambwani, K, Sahni, A., Kar, R.K., Dutta, D., 2003. Oldest known non-marine diatoms (Aulacoseira) from the uppermost Cretaceous Deccan Intertrappean beds and Lameta Formation of India. Revue de Micropaléontologie, 46 (2), 67-71.

Arai, H., Fukushima, T., 2012. Silicon budget of eutrophic Lake Kasumigaura, Japan. Journal of Soils Sediments, 12, 1501–1507.

Arbey, F., 1980. Les formes de la silice et l'identification des evaporites dans les formations silicifiées. (Silica forms and evaporite identification in cherts). Bulletin des Centres de Recherches Exploration-Production Elf-Aquitaine, 4, 1, 309-365.

Aslanian, D., Moulin, M., Olivet, J.L., Unternehr, P., Matias, L., Bache, F., Rabineau, M., Nouzé, H., Klingelheofer, F., Contrucci, I., Labails, C., 2009. Brazilian and African passive margins of the central segments of the South Atlantic. Tectonophysics, 468, 98–112.

Bate, R.H., 1999. Non-marine ostracod assemblages of the Pre-Salt rift basins of West Africa and their role in sequence stratigraphy. In: Cameron, N.R., Bate, R.H., Clure, V.S. (Eds), The Oil and Gas Habitats of the South Atlantic. Geological Society, London, Special Publications, 152, 283–292.

Bate, R.H., Cameron, N.R., Brandao, M.G.P., 2001. The Lower Cretaceous (Pre-Salt) lithostratigraphy of the Kwanza Basin, Angola. Newsletters of Stratigraphy, 38, 117–127.

Beglinger, S.E., Doust, H., Cloetingh, S., 2012. Relating petroleum system and play development to basin evolution: West African South Atlantic basins. Marine and Petroleum Geology, 30, 1–25.

Behr, H.J., Röhricht, C., 2000. Record of seismotectonic events in siliceous cyanobacterial sediments (Magadi cherts), Lake Magadi, Kenya. International Journal of Earth Sciences, 89, 268–283.

Blanc, P., Lassin, A., Piantone, P., Azaroual, M., Jacquemet, N., Fabbri, A., Gaucher, E.C., 2012. Thermoddem: a geochemical database focussed on low temperature water/rock interactions and waste materials. Applied Geochemistry 27, 2107-2116. Available at: hhtp://Thermoddem.brgm.fr/

Bottinga, Y., Craig, H., 1969. Oxygen isotope fractionation between CO_2 and water, and the isotopic composition of marine atmospheric CO_2. Earth and Planetary Science Letters, 5, 285-295.

Brice, S.E., Cochran, M.D., Pardo, G., Edwards, A.D., 1982. Tectonics and sedimentation of the South Atlantic rift sequence: Cabinda, Angola. In: Watkins, J.S., Drake, C.L. (Eds), Studies in Continental Margin Geology. American Association of Petroleum Geologists Memoirs, 34, 5–18.

Brunet, R.D., Bustillo, M.A., 2014. Exeptional silica speleothems in a volcanic cave: A unique example of silicifications and sub-aquatic opaline stromatolite formation (Terceira, Azores). Sedimentology, 61 (7), 2113–2135.

Bustillo, M.A., 2010. Silicification of continental carbonates. Developments in Sedimentology, 62, 153–178.

Bustillo, M.A., Alonso-Zarza, A.M., 2007. Overlapping of pedogenesis and meteoric diagenesis in distal alluvial and shallow lacustrine deposits in the Madrid Miocene Basin, Spain. Sedimentary Geology, 198, 255–271.

Bustillo, M.A., Pérez-Jiménez, J.L., Alonso-zarza, A.M., Furio, M., 2012. Moganite in the chalcedony varieties of continental cherts (Miocene, Madrid Basin, Spain). Spectroscopy Letters, 45 (2), 109–113.

Bustillo, M.A., Armenteros, I., Huerta, P., 2017. Dolomitization, gypsum calcitization and silicification in carbonate-evaporite shallow lacustrine deposits. Sedimentology, 64 (4), 1147-1172.

Cammack, J.N., Spicuzza, M.J., Cavosie, A.J., Van Kranendonk, M.J., Hickman, A.H., Kozdon, R., Orland, I.J., Kitajima, K., Valley, J.W., 2018. SIMS Microanalysis of the Strelley Pool Formation Cherts and the Implications for the Secular-Temporal Oxygen-isotope Trend of Cherts. Precambrian Research 304, 125-139.

Cangemi, M., Bellanca, A., Borin, S., Hopkinson, L., Mapelli, F., Neri, R., 2010. The genesis of actively growing siliceous stromatolites: Evidence from Lake Specchio di Venere, Pantelleria Island, Italy. Chemical Geology, 276, 318–330.

Carminatti, M., Wolff, B., Gamboa, L., 2008. New Exploratory Frontiers in Brazil: Proceedings of the 19th World Petroleum Congress. Spain, Madrid. June 29-July 3, 2008, 11 pp.

Cerling, T.E., 1994. Chemistry of closed basin lake waters: a comparison between African Rift Valle and some centra North American rivers and lakes. In: Gierlowski-

Kordesch, E.H., Kelts, K. (Eds). The Global Geological Record of Lake Basins. Cambridge University Press, Cambridge, 29–30.

Chaboureau, A.C., Donnadieu, Y., Sepulchre, P., Robin, C., guillocheau, F., Rohais, S., 2012. The Aptian evaporites of the South Atlantic : a climatic paradox ? Climate of the Past Discussions, 8, 121-144.

Chaboureau, A.C., Guillocheau, F., Robin, C., Rohais, S., Moulin, M., Aslanian, D., 2013. Paleogeographic evolution of the central segment of the South Atlantic during Early Cretaceous times: paleotopographic and geodynamic implications. Tectonophysics 604, 191–223.

Chavagnac, V., Monnin, C., Ceuleneer, G., Boulart, C., Hoareau, G., 2013. Characterization of hyperalkaline fluids produced by low-temperature serpentinization of mantle peridotites in the Oman and Ligurian ophiolites. Geochemistry Geophysics Geosystems, 14, 2496–2522.

Chen, Z., Yan, H., Li, j., Zhang, G., Zhang, Z., Liu, B., 1999. Relationship between Tertiary volcanic rocks and hydrocarbons in the Liaohe Basin, People's Republic of China. American Association of Petroleum Geologists Bulletin, 83, 1004–1014.

Clayton, R.N., Steiner, A., 1975. Oxygen isotope studies of the geothermal system at Wairakei, New Zealand. Geochimica et Cosmochimica Acta, 39, 1179-1186.

Clayton, R.N., O'Neil, J.R., Mayeda, T.K., 1972. Oxygen isotope exchange between quartz and water. Journal of geophysical research, 77(17), 3057-3067.

Comin-Chiaramonti, P., Gomes, C.B., Cundari, A., Castorina, F., Censi, P., 2007. A review of carbonatitic magmatism in the Parana-Angola-Namibia (PAN) system. Periodico di Mineralogia, 76 (2-3), 25-78.

Comin-Chiaramonti, P., De Min, A., Girardi, V.A.V., Ruberti, E., 2011. Post-paleozoic Magmatism in Angola and Namibia: a Review. The Geological Society of America. Special Paper 478, 233-246.

Cornwell, J.C., Banahan, S., 1992. A silicon budget for an Alaskan artic lake. Hydrobiologia, 240, 37–44.

Coterill, K., Tari, G.C., Molnar, J., Ashton, P.R., 2002. Comparison of depositional sequences and tectonic styles among the West African deepwater frontiers of western Ivory Coast, southern Equatorial Guinea, and northern Namibia. Leading Edge, 21, 1103–1111.

Couturié, J.P., 2015. Cadre géologique de la Limagne et genèse du bitumen. Le Règne Minéral — hors-série 21, 15-22.

Craig, H., Boato, G., White, D.E., 1956. Isotopic geochemistry of thermal waters. In: Proceedings of the Conference on Nuclear Processes in Geological Settings. 2nd National Academy of Science National Research Council Publication.

Criss, R.E., 1999. Principles of Stable Isotope Distribution. Oxford University Press, New York. 264 pp.

Degens, E.T., Epstein, S., 1962. Relationship between O^{18}/O^{16} ratios in coexisting carbonates, cherts, and diatomites. American Association of Petroleum Geologists, 46, 534–542.

Dekov, V.M., Egueh, N.M., Kamenov, G.D., Bayon, G., Lalonde, S.V., Schmidt, M., Liebetrau, V., Munnik, F., Fouquet, Y., Tanimizu, M., Awaleh, M.O., Guirreh, I., Le Gall, B., 2014. Hydrothermal carbonate chimneys from a continental rift (Afar Rift): Mineralogy, geochemistry, and mode of formation. Chemical Geology, 387, 87–100.

DeMaster, D.J., 1981. The supply and accumulation of silica in the marine environment. Geochimica et Cosmochimica Acta, 45, 1715-1732.

Denis M., Kluska J.M., 2017. South Kwanza basin (Offshore Angola) as a major cornerstone of West African margin. Abstract American Association of Petroleum Geologists ACE Conference, April 2017, Houston Texas.

Denny, A.C., Kozdon, R., Kitajima, K., Valley, J.W., 2017. Isotopically Zoned Carbonate Cements in Early Paleozoic Sandstones of the Illinois Basin: $\delta^{18}O$ and $\delta^{13}C$ Records of Burial and Fluid Flow. Sedimentary Geology, 361, 93-110.

Deocampo, D.M., 2005. Evaporitive evolution of surface waters and the role of aqueous CO2 in magnesium silicate precipitation: Lake Eyasi and Ngorongoro Crater, northern Tanzania. South African Journal of Geology, 108, 493-504.

Deocampo, D.M., Renaut, R.W., 2016. Geochemistry of African Soda Lakes. In: Schagerl, M., (Ed) Soda Lakes of East Africa. Springer, Cham.

Devouard, B., Bornet, R., 2015. Vous avez dit lussatite? Le Règne Minéral — hors-série 21, 51-54.

Dickson, J.A.D., 1966. Carbonate identification and genesis as revealed by staining. Journal of Sedimentary Petrology, 36, 491–505.

Dickson, J.A.D., 1991. Disequilibrium carbon and oxygen isotope variations in natural calcite. Nature, 353, 842–844.

Dingle, R.V. 1999. Walvis Ridge barrier: Its influence on palaeoenvironments and source rock generation deduced from ostracod distributions in the early South Atlantic Ocean. In: Cameron, N.R., Bate, R.H., Clure, V.S. (Eds), The Oil and Gas Habitats of the South Atlantic. Geological Society, London, Special Publications, 153, 293–302.

Dunkley, P.N., Smith, M., Allen, D.J., Darling, W.G., 1993. The geothermal activity and geology of the northern sector of the Kenya Rift Valley. British Geological Survey Research Report SC/93/1, 185 pp.

Eiler, J.M., Graham, C., Valley, J.W., 1997. SIMS analysis of oxygen isotopes: matrix effects in complex minerals and glasses. Chemical Geology, 138, 221–244.

Ernst, W.G., Calvert, S.E., 1969. An experimental study of the recrystallization of porcelanite and its bearing on the origin of some bedded cherts. American Journal of Science, 267, 114–133.

Eugster, H.P., 1967. Hydrous sodium silicates from Lake Magadi, Kenya: Precursors of bedded chert. Science, 157, 1177–1180.

Eugster, H.P., 1969. Inorganic bedded cherts from the Magadi area, Kenya. Contributions to Mineralogy and Petrology, 22 (1), 1–31.

Eugster, H.P., Jones, B.F., 1968. Gels composed of sodium aluminium silicate, Lake Magadi, Kenya. Science, 161, 160–164.

Ewers, G.R., 1991. Oxygen isotopes and the recognition of siliceous sinters in epithermal ore deposits. Economic Geology, 86, 173–178.

Flörke, O.W., Köhler-Herbertz, B., Langer, K., Tönges, I., 1982. Water in microcrystalline quartz of volcanic origin: agates. Contribution to Mineralogy and Petrology, 80, 324–333.

Folk, R.L., Pittman, J.S., 1971. Length-slow chalcedony: a new testament for vanished evaporites. Journal of sedimentary research, 41, 1045–1048.

Föllmi, K.B., 2012. Early Cretaceous life, climate and anoxia. Cretaceous Research, 35, 230–257.

Foubert, A., Jaramillo-Vogel, D., Held, A.-E., Camoin, C., Virgone, A., 2014. Diagenesis of Cretaceous pre-salt deposits: Namibe and Benguela Basins (Angola). Fribourg, Switzerland. Unpublished report, funded by Total (FR00005140/FR00005813).

Fouillac, A.M., Girard, J.-P., 1996. Laser oxygen isotope analysis of silicate/oxide grain separates: evidence for a grain size effect? Chemical Geology, 130, 31–54.

Frixa, A., Maragliulo, C., Consonni, A., Ortenzi, A., 2014. Dolomitization of the lacustrine carbonates of the Toca Fm. (Kambala Field, Offshore Cabienda) and quantitative diagenetic modeling. Society of Petroleum Engineers. SPE-171960-MS. Doi: 10:2118/171960-MS.

Gao, G., Land, L., 1991. Nodular chert from the Arbuckle Group, Slick Hills, SW Oklahoma: a combined field, petrographic and isotopic study. Sedimentology, 38, 857–870.

Garcia-Romero, E., Vegas, J., Baldonedo, J.L., Marfil, R., 2005. Clay minerals as alteration products in basaltic volcaniclastic deposits of La Palma (Canary Island, Spain). Sedimentary Geology, 174, 237–253.

García-Ruiz, J.M., 2000. Geochemical scenarios for the precipitation of biomimetic inorganic carbonates. In: Grotzinger, J., James, N. (Eds), Carbonate sedimentation and diagenesis in the evolving Precambrian world. Society for Sedimentary Geology special publication 67, 75–89.

Gindre-Chanu, L., Warren, J.K., Puigdefabregas, C., Sharp, I.R., Peacock, D.P., Swart, R., Poulsen, R., Ferreira, H., Henrique, L., 2015. Diagenetic evolution of Aptian evaporites in the Namibe Basin (south-west Angola). Sedimentology, 62, 204–233.

Gindre-Chanu, L., Perri, E., Sharp, I.R., Peacock, D.C.P., Swart, R., Poulsen, R., Ferreira, H., Machado, V., 2016. Origin and diagenetic evolution of gypsum and microbialitic carbonates in the Late Sag of the Namibe Basin (SW Angola). Sedimentary Geology, 342, 133–153.

Girard, J.P., San Miguel, G., 2017. Evidence of high temperature regimes in the Pre-Salt series, Kwanza Basin, Offshore Angola. Abstract American Association of Petroleum Geologists ACE Conference, April 2017, Houston Texas.

Girard, J.P., Munz, I.A., Johansen, H., Hill, S., Canham, A., 2001. Conditions and timing of quartz cementation in Brent reservoirs, Hild Field, North Sea: constraints from fluid inclusions and SIMS oxygen isotope microanalysis. Chemical Geology, 176, 73–92.

Girard, J-P., San Miguel, G., Godeau, N., Deschamps, P., 2017. An integrated study of a case of complex hydrothermal diagenesis in a PreSalt reservoir offshore Angola. Goldschmidt Conference, 13-18 August, Paris, France

Giresse, P., 2005. Mesozoic-Cenozoic history of the Congo Basin. Journal of African Earth Sciences, 43, 301–315.

Goldberg, K., Kuchle, J., Scherer, C., Alvarenga, R., Ene, P.L., Armelenti, G., De Ros, L.F., 2017. Re-sedimented deposits in the rift section of the Campos Basin. Marine and Petroleum Geology, 80, 412–431.

Gomes, P.O., Kilsdonk, B., Minken, J., Grow, T., Barragan, R., 2009. The Outer High of the Santos Basin, southern São Paulo Plateau, Brazil: Pre-Salt exploration outbreak, paleogeographic setting, and evolution of the syn-rift structures. American Association of Petroleum Geologists Search and Discovery Article #10193.

Gonfiantini, R., 1986. Environmental isotopes in lake studies. In: Fritz, P., Fontes, J. (Eds), Handbook of environmental isotope geochemistry, vol 2. Elsevier, Amsterdam, 112–168.

Guidry, S.A., Chafetz, H.S., 2003. Anatomy of siliceous hot springs: examples from Yellowstone National Park, Wyoming, USA. Sedimentary Geology, 157, 71–106.

Guiraud, M., Buta-Neto, A., Quesne, D., 2010. Segmentation and differential post-rift uplift at the Angola margin as recorded by the transform-rifted Benguela and oblique-to-orthogonal-rifted Kwanza basins. Marine and Petroleum Geology, 27, 1040–1068.

Guiraud, R., Maurin, J.-C., 1991. Le Rifting en Afrique au Crétacé inferieur; synthèse structurale, mise en évidence de deux étapes dans la genèse des bassins, relations avec

les ouvertures océaniques péri-africaines. Bulletin de la Société Géologique de France, 162, 811-823.

Harris, C., 1989. Oxygen-isotope zonation of agates from Karoo volcanics of the Skeleton Coast, Namibia. American Mineralogist, 74, 476–481.

Harris, N.B., 2000. The Toca Carbonate, Congo Basin: response to an evolving rift lake. In: Mello, M.R., Katz, B.J. (Eds), Petroleum systems of South Atlantic margins. American Association of Petroleum Geologists Memoir 73, 341–360.

Hawkesworth, C.J., Gallagher, K., Kelley, S., Mantovani, M., Peate, D.W., Regelous, M., Rogers, N.W., 1992. Parana magmatism and the opening of the south Atlantic. In: Storey, B.C., Alabaster, R.J., Pankhurst, R.J. (Eds.), Magmatism and the Causes of Continental Breakup, vol. 68. Geological Society Special Publication, 221–240.

Heaney, P.J., 1993. A proposed mechanism for the growth of chalcedony. Contribution to Mineralogy and Petrology, 115, 66–74.

Heath, G.R., 1974. Dissolved silica and deep-sea sediments. In: Hay, W.W. (Ed), Studies in Paleo-Oceanography. Society for sedimentary geology, 20, 77–93.

Heine, C., Zoethout, J., Muller, D., 2013. Kinematics of the South Atlantic rift. Solid Earth, 4, 215–253.

Herzig, P.M., Becker, K.P., Stoffers, P., Bäcker, H., Blum, N., 1988. Hydrothermal silica chimney fields in the Galapagos Spreading Center at 86°W. Earth and Planetary Science Letters, 89, 261–272.

Hesse, R., 1988. Origin of chert I: Diagenesis of biogenic siliceous sediments. Geoscience Canada, 15 (3), 171–192.

Hesse, R., 1989. Silica Diagenesis: Origin of Inorganic and Replacement Cherts. Earth-Science Reviews, 26, 253–284.

Hoefs, J., 2009. Stable Isotope Geochemistry. Springer-Verlag Berlin Heidelberg. 244 pp.

Hu, G., Clayton, R.N., 2003. Oxygen isotope salt effects at high pressure and high temperature and the calibration of oxygen isotope geothermometers. Geochimica et Cosmochimica Acta, 67(17), 3227-3246.

Iler, R.K., 1979. The chemistry of Silica: solubility, polymerization, colloid and surface properties and biochemistry of silica. John Wiley and Sons, Chichester, 896 pp.

Jackson, M.P.A., Cramez, C., Fonck, J.M., 2000. Role of subaerial volcanic rocks and mantle plumes in creation of South Atlantic margins: implications for salt tectonics and source rocks. Marine and Petroleum Geology, 17(4), 477–498.

Jones, B., Renaut, R.W., 2003. Hot spring and geyser sinter: the integrated product of precipitation, replacement, and deposition. Canadian Journal of Earth Science, 40, 1549–1569.

Jones, B., Renaut, R.W., 2010. Impact of seasonal changes on the formation and accumulation of soft siliceous sediments on the discharge apron of Geysir, Iceland. Journal of Sedimentary Research, 80, 17–35.

Jones, B.F., Rettig, S.L., Eugster, H.P., 1967. Silica in alkaline brines. Science, 158, 1310–1314.

Jones, G.D., Xiao, Y., 2013. Geothermal convection in South Atlantic pre-salt lacustrine carbonates: Developing diagenesis and reservoir quality predictive concepts with reactive transport models. American Association of Petroleum Geologists Bulletin, 97(8), 1249–1271.

Jourdan, A.-L., Vennemann, T.W., Mullis, J., Ramseyer, K., 2009. Oxygen isotope sector zoning in natural hydrothermal quartz. Mineralogical Magazine, 73(4), 615–632.

Karner, G.D., Driscoll, N.W. 1999. Tectonic and stratigraphic development of the West Africa and eastern Brazilian margins: Insights from quantitative basin modelling. In:

Cameron, N.R., Bate, R.H., Clure, V.S. (Eds) The Oil and Gas Habitats of the South Atlantic. Geological Society, London, Special Publications, 153, 11–40.

Karner, G.D., Driscoll, N.W., Barker, D.H.N., 2003. Syn-rift regional subsidence across the West African continental margin: the role of lower plate ductile extension. Geological Society, London, Special Publication, 207, 105–129.

Kempe, S., Degens, E.T., 1985. An early soda ocean? Chemical geology, 53, 95–108.

Knauth, L.P., 1994. Petrogenesis of cherts. In: Heyney, P.J., Prewitt, C.T., Gibbs, G.V. (Eds.), Silica: Physical behaviour, geochemistry and materials applications. Reviews in Mineralogy, 29, 233–258.

Knauth, L.P., Epstein, S., 1975. Hydrogen and oxygen isotope ratios in silica from the joides deep sea drilling project. Earth and Planetary Science Letters, 25, 1–10.

Knauth, L.P., Epstein, S., 1976. Hydrogen and oxygen isotope ratios in nodular and bedded cherts. Geochimica et Cosmochimica Acta, 40, 1095-1108.

Knauth, L.P., Lowe, D.R., 1978. Oxygen isotope geochemistry of cherts from Onverwacht Group (3.4 bilion years), Transvaal, South Africa with impocations for secular variations in the isotopic compositions of cherts. Earth and Planetary Science Letters, 41, 209–222.

Kolodny, Y., Epstein, S., 1976. Stable isotope geochemistry of deep sea cherts. Geochimica et Cosmochimica Acta, 40, 1195-1209.

Krebs, W., Gladenkov, A.Y., Jones, G., D., 2010. Diatoms in oil and gas expoloration. In: Smol, J.P., Stoermer, E.F. (Eds), The diatoms: applications for the environmental and earth sciences, 2nd edition. Cambridge University Press, Cambridge.

Larkin, J.J., Armigton, A.F., O'Connor, J.J., Lipson, H.G., Horrigan, J.A., 1982. Growth of quartz with high aluminium concentration. Journal of Crystal Growth, 60, 136–140.

Lee, H., Muirhead, J.D., Fischer, T.P., Ebinger, C.J. Kattenhorn, S.A., Sharp, Z.D., Kianji, G., 2016. Massive and prolonged deep carbon emissions associated with continental rifting. Nature geoscience, 9, 145-149.

Leleu, T., Chavagnac, V., Delacour, A., Noiriel, C., Ceuleneer, G., Aretz, M., Rommevaux, C., Ventalon, S., 2016. Travertines associated with hyperalkaline springs: evaluation as a proxy for palaeoenvironmental conditions and sequestration of atmospheric CO_2. Journal of Sedimentary Research, 86, 1328–1343.

Livingstone, D.A., 1963. Chemical composition of rivers and lakes. USGS professional paper 440-G, 61 pp.

Lynne, B.Y., Campbell, K.A., Moore, J.N., Browne, P.R.L., 2005. Diagenesis of 1900-year-old siliceous sinter (opal-A to quartz) at Opal Mound, Roosevelt Hot Springs, Utah, USA. Sedimentary Geology, 179 (3–4), 249–278.

Mackenzie, F.T., Garrels, R.M., Bricker, O.P., Bickley, F., 1967. Silica in Sea Water: control by silica minerals. Science, 155 (3768), 1404–1405.

Maliva, R.G., Knoll, A.H., Siever, R., 1989. Secular change in chert distribution: A reflection of evolving biological participation in the silica cycle. Palaios, 4, 519–532.

Marin, J., 2009. Composition isotopique de l'oxygène et du silicium dans les cherts Précambriens : Implications Paléo-environnementales. PhD thesis, Institut National Polythechnique de Lorraine, 402 pp.

Marin, J., Chaussidon, M., Robert, F., 2010. Microscale oxygen isotope variations in 1.9 Ga Gunflint cherts: Assessments of diagenesis effects and implications for oceanic paleotemperature reconstructions. Geochimica et Cosmochimica Acta, 74, 116-130.

Marin-Carbonne, J., Chaussidon, M., Boiron, M.C., Robert, F., 2011. A combined in situ oxygen, silicon isotopic and fluid inclusion study of a chert sample from Onverwacht

Group (3.35 Ga, South Africa): New constraints on fluid circulation. Chemical Geology, 286, 59–71.

Marin-Carbonne, J., Robert, F., Chaussidon, M., 2014. The silicon and oxygen isotope compositions of Precambrian cherts: a record of oceanic paleo-temperatures? Precambrian research, 247, 223–234.

Marzoli, A., Melluso, L., Morra, V., Renne, P.R., Sgrosso, I., D'Antonio, M., Duarte- Morais, L., Morais, E.A.A., Ricci, G., 1999. Geochronology and petrology of Cretaceous basaltic magmatism in the Kwanza basin (western Angola) and relationships with the Parana-Etendeka continental basalt province. Journal of Geodynamics, 28, 341–356.

Matsuhisa, Y., Goldsmith, J.R., Clayton, R.N., 1979. Oxygen isotopic fractionation in the system quartz-albite-anorthite-water. Geochimica et Cosmochimica Acta, 43 (7), 1131-1140.

Matthews, K.J., Müller, R.D., Wessel, P., Whittaker, J.M., 2011. The tectonic fabric of the ocean basins. Journal of Geophysical Research—Solid Earth, 116, B12109.

McBride, E.F., Abdel-Wahab, A., El-Younsy, A.R.M., 1999. Origin of spheroidal chert nodules, Drunka Formation (Lower Eocene), Egypt. Sedimentology, 46, 733–755.

McCall, J., 2010. Lake Bogoria, Kenya: Hot and warm springs, geysers and Holocene stromatolites. Earth-Science Reviews, 103, 71–79.

Mercedes-Martín, R., Rogerson, M.R., Brasier, A.T., Vonhof, H.B., Prior, T.J., Fellows, S.M., Reijmer, J.J.G., Billing, I., Pedley, H.M., 2016. Growing spherulitic calcite grains in saline, hyperalkaline lakes: experimental evaluation of the effects of Mg-clays and organic acids. Sedimentary Geology, 335, 93–102.

Meyers, W.J., 1977. Chertification in the Mississippian Lake Valley Formation, Sacramento Mts., New Mexico. Sedimentology, 25, 105–124.

Michalopoulos, P., Aller, R.C., 1995. Rapid clay mineral formation in Amazon delta sediments: Reverse weathering and oceanic elemental cycles. Science, 270 (5236), 614–617.

Michalopoulos, P., Aller, R.C., 2004. Early diagenesis of biogenic silica in the Amazon delta: alteration, authigenic clay formation, and storage. Geochimica et Cosmochimica Acta, 68 (5), 1061-1085.

Miliken, K.L., 1979. The silicified evaporite syndrome—two aspect of silicifications history of former evaporate nodules from southern Kentucky and northern Tennessee. Journal of Sedimentary Petrology, 49 (1), 245–256.

Millot, G., 1970. Geology of Clays: weathering, sedimentology, geochemistry. Springer-Verlag: London.429 pp.

Moore, T.C., Jr, Rabinowitz, P.D., Borella, P.E., Shackleton, N.J. & Boersma, A. 1984. History of the Walvis Ridge. In: Moore, T.C., Jr, Rabinowitz, P.D., Borella, P., Boersma, A., Shackleton, N.J., Initial Reports of the Deep Sea Drilling Project, Volume 74. United States Government Printing Office, Washington, DC, 873–894.

Moulin, M., Aslanian, D., Unternehr, P., 2010. A new starting point for the south Atlantic and Equatorial Atlantic Ocean. Earth-Science Review, 98, 1–37.

Nürnberg, D., Müller, R.D. 1991. The tectonic evolution of the South Atlantic from Late Jurassic to present. Tectonophysics, 191, 27–53.

O'Connor, J.M. & Duncan, R.A. 1990. Evolution of the Walvis Ridge—Rio Grande Rise hot spot system: Implications for African and South American plate motions over plumes. Journal of Geophysical Research, 95, 17475–17502.

O'Neil, J.R., Hay, R.L., 1973. $^{18}O/^{16}O$ ratios in cherts associated with the saline lake deposits of East Africa. Earth and Planetary Science Letters, 19, 257–266.

Pereira, E., 1969. Nota sobre os vulcanitos neocretacicos de Egito-Praia (entre Novo Redondo e Lobito). Boletim dos serviços de Geologia e Minas, Luanda.

Pereira, E., 1971. Nota sobre o complexo ígneo ante-apciano do Cuanza-sul. Boletim Dos serviços de Geologia e Minas 23, 51-80. Luanda.

Peron-Pinvidic, G., Manatschal, G., Masini, E., Sutra, E., Flament, J.M., Haupert, I., Unternehr, P., 2015. Unravelling the Along-strike Variability of the Angola-Gabon Rifted Margin: a Mapping Approach. In: Sabato Ceraldi, T., Hodgkinson, R.A., Backe, G. (Eds.), Petroleum Geoscience of the West Africa Margin. Geological Society, London Special Publications, 438.

Pindell, J.L., 1995. Circum-Caribbean sedimentary basin development and timing of hydrocarbon maturation as a function of Caribbean plate tectonic evolution. In Miller, R.L., Escalante, G., Reinemund, J.A., Bergin, M.J. (Eds.), Energy and Mineral Potential of the Central American-Caribbean Regions: Berlin, Springer, p. 47–56.

Pinto, V.H.G., Manatschal, G., Karpoff, A.M., Ulrich, M., Viana, A.R., 2017. Seawater storage and element transfer associated with mantle serpentinization in magma-poor rifted margins: a quantitative approach. Earth and Planetary Science Letters, 459, 227–237.

Pittari, A., Muir, S.L., Hendy, C.H., 2016. Lake-floor sediment texture and composition of a hydrothermally-active, volcanic lake, Lake Rotomahana. Journal of volcanology and geothermal research, 314, 169–181.

Pletsch, T., Erbacher, J., Holbourn, A.E.L., Kuhnt, W., Moullade, M., Oboh-Ikuenobede, F.E., Söding, E., Wagner, T., 2001. Cretaceous separation of Africa and South America: the view from the West African margin (ODP Leg 159). Journal of South American Earth Sciences, 14, 147–174.

Pokrovsky, O.S., Schott, J., 2001. Kinetics and mechanism of dolomite dissolution in neutral to alkaline solutions revisited. American Journal of Science, 301, 597–626.

Poros, Z., Jagniecki, E., Luczaj, J., Kenter, J., Gal, B., Correa, T.S., Ferreira, E., Heumann, M., Elifritz, A., Johnston, M., McFadden, K.A., Matt, V., 2017. Origin of silica in Pre-Salt carbonates, Kwanza Basin, Angola. Abstract American Association of Petroleum Geologists ACE Conference, April 2017, Houston Texas.

Quirk, D.G., Hertle, M., Jeppesen, J.W., Raven, M., Mohriak, W.U., Kann, D.J., Nørgaard, M., Howe, M.J., Hsu, D., Coffey, B., Mendes, M.P. 2013. Rifting, subsidence and continental break—up above a mantle plume in the central South Atlantic. In: Mohriak, W.U., Danforth, A., Post, P.J., Brown, D.E., Tari, G.C., Nemcok, M., Sinha, S.T. (Eds) Conjugate Divergent Margins. Geological Society, London, Special Publications, 369, 185–214

Renaut, R.W., Jones, B., Tiercelin, J.J., 1998. Rapid *in situ* silicifications of microbes at Loburu hot springs, Lake Bogoria, Kenya Rift Valley. Sedimentology, 45, 1083–1103.

Renaut, R.W., Jones, B., Le Turdu, C., 1999. Calcite lilypads and ledges at Lorusio Hot Springs, Kenya Rift Valley: travertine precipitation at the air-water interface. Canadian Journal of Earth Sciences, 46, 649–666.

Renaut, R.W., Jones, B., Tiercelin, J.J., Tarits, C., 2002. Sublacustrine precipitation of hydrothermal silica in rift lakes: evidence from Lake Baringo, central Kenya Rift Valley. Sedimentary Geology, 148, 235–257.

Riech, V., v. Rad, U., 1979. Silica diagenesis in the Atlantic Ocean: Diagenetic potential and trasformations. In: Talwani, M., Hay, W., Ryan, W.B.F. (Eds.), Deep drilling results in the Atlantic Ocean: Continental margins and paleoenvironment. American Geophysical Union, Maurice Ewing Series, 3, 315–341.

Rimstidt, J.D., 1997. Quartz solubility at low temperatures. Geochimica et Cosmochimica Acta, 61 (13), 2553-2558.

Risacher, F., 1978. Le cadre géochimique des bassins à evaporites des Andes Boliviennes. Cahier ORSTOM., Séries Géologiques, 10 (1), 37-48.

Saller, A., Rushton, S., Buambua, L., Inman, K., McNeil, R., Dickson, J.A.D., 2016. Presalt stratigraphy and depositional systems in the Kwanza Basin, offshore Angola. American Association of Petroleum Geologists Bulletin, 100 (7), 1135–1164.

San Miguel, G., Teboul, P.A., Virgone, A., Barbat, L., Girard, J.P., 2017. A review of carbonate continental systems in active rift settings (Offshore Angola) – a combined subsurface and outcrop study for derisking reservoir presence. Abstract American Association of Petroleum Geologists ACE Conference, April 2017, Houston Texas.

Schmidt, P., Slodczyk, A., Léa, V., Davidson, A., Puaud, S., Sciau, P., 2013. A comparative study of the thermal behaviour of length-fast chalcedony, length-slow chalcedony (quartzine) and moganite. Physics and Chemistry of Minerals, 40, 331–340.

Schröder, S., Ibekwe, A., Saunders, M., Dixon, R., Fisher, A., 2016. Algal-microbial carbonates of the Namibe Basin (Albian, Angola): implications for microbial carbonate mound development in the South Atlantic. Petroleum Gescience, 22, 71–90.

Seton, M., Wittaker, J.,M., Wessel, P., Müller, R.D., DeMets, C., Merkouriev, S., Cande, S., Gaina, C., Eagles, G., Granot, R., Stock, J., Wright, N., Williams, S.E., 2014. Community infrastructure and repository for marine magnetic identifications. Geochemistry, Geophysics, Geosystems, 15, 1629–1641.

Shackleton, N.J., Kennett, J.P., 1975. Paleotemperature history of the Cenozoic and the initiation of Antartic glaciations: oxygen and carbon isotope analyses in DSDP sites 277, 279, and 281. In: Kennett, J.P., Houtz, R.E. (Eds) Initial reports of the Deep Sea Drilling Project, Washington, 743-755.

Shanks, W.C., Alt, J.C., Morgan, L.A., 2007. Geochemistry of sublacustrine hydrothermal deposits in Yellowstone Lake—Hydrothermal reactions, stable isotope systematics, sinter deposition, and spire formation. In: Morgan, L.A. (Ed), Integrated geoscience studies in the Greater Yellowstone Area—Volcanic, tectonic, and hydrothermal processes in the Yellowstone geoecosystem. United States Geological Survey Professional paper 1717.

Sharp, Z.D., Gibbons, J.A., Maltsev, O., Atudorei, V., Pack, A., Sengupta, S., Shock, E.L., Knauth, L.P., 2016. A calibration of the triple oxygen isotope fractionation in the SiO_2-H_2O system and applications to natural samples. Geochimica et Cosmochimica Acta, 186, 105-119.

Sheppard, S.M.F., 1986. Characterization and isotopic variations in natural waters. In: Valley, J.W., Taylor, H.P. Jr., O'Neil, J.R. (Eds.) Stable isotopes in high temperature geological processes. Reviews in Mineralogy V. 16, Mineralogical Society of America, Chelsea, 165-183.

Sims, P.A., Mann, D.G., Medlin, L.K., 2006. Evolution of the diatoms: insights from fossil, biological and molecular data. Phycologia, 45, 361–402.

Smrzka, D., Kraemer, S.M., Zwicker, J., Birgel, D., Fisher, D., Kasten, S., Goedert, J.L., Peckmann, J., 2015. Constraining silica diagenesis in methan-seep deposits. Palaeogeography, Palaeoclimatology, Palaeoecology, 420, 13–26.

Souza-Egipsy, V., Wierzchos, J., Ascaso, C., Nealson, K.H., 2005. Mg-silica precipitation in fossilization mechanisms of sand tufa endolithic microbial community, Mono Lake (California). Chemical Geology, 217 (1–2), 77–87.

Spötl, C., Wright, V.P., 1992. Groundwater dolocretes from the Upper Triassic of the Paris Basin, France: a case study of an arid, continental diagenetic facies. Sedimentology, 39, 1119–1136.

Sturchio, N.C., Dunkley, N., Smith, M., 1993. Climate-driven variations in geothermal activity in the northern Kenya rift valley. Nature, 362, 233–234.

Sylvestre, F., Servant-Vildary, S., Roux, M., 2001. Diatom-based ionic concentration and salinity models from the south Bolivian Altiplano (15–23°S). Journal of Paleolimnology, 25, 279–295.

Szatmari, P., Milani, E.J., 2016. Tectonic control of the oil-rich large igneous-carbonate-salt province of the South Atlantic rift. Marine and Petroleum Geology, 77, 567–596.

Taran, Y.A., Hedenquist, J.W., Korzhinsky, M.A., Tkachenko, S.I., Shmulovich, K.I., 1995. Geochemistry of magmatic gases from kudryavy volcano, Iturup, Kuril Islands. Geochemica et Cosmochimica Acta, 59 (9), 1749-1761.

Teboul, P.-A., Durlet, C., Gaucher, E.C., Virgone, A., Girard, J.-P., Curie, J., Lopez, B., Camoin, G.F., 2016. Origins of elements building travertine and tufa: New perspectives provided by isotopic and geochemical tracers. Sedimentary Geology, 334, 97–114.

Teboul, P.-A., Kluska, J.M., Marty, N.C.M., Debure, M., Durlet, C., Virgone, A., Gaucher, E.C., 2017. Volcanic rock alterations of the Kwanza Basin, offshore Angola—Insights from an integrated petrological, geochemical and numerical approach. Marine and Petroleum Geology, 80, 394–411.

Teisserenc, P., Villemin, J. 1990. Sedimentary basin of Gabon—Geology and oil systems. In: Edwards, J.D., Santogrossi, P.A. (Eds), Divergent/Passive Margin Basins. American Association of Petroleum Geologists Memoirs, 48, 117–199.

Terra, G.J.S., Spadini, A.R., França, A.B., Sombra, C.L., Zambonato, E.E., da Silva Juschaks, L.C., Arienti, L.M., Erthal, M.M., Blauth, M., Franco, M.P., Matsuda, N.S., da Silva, N.G.C., Moretti Junior, P.A., D'Avila, R.S.F., de Souza, R.S., Tonietto, S.N., Couto dos Anjos, S.M., Campinho, V.S., Winter, W.R., 2010. Classificação de

rochas carbonáticas aplicável às bacias sedimentares brasileiras. Bulletin Geoscience Petrobras, Rio de Janeiro 18 (1), 9–29.

Thiry, M., Maréchal, B., 2001. Development of thightly cemented sandstone lenses in uncemented sand: exemple of the Fontainebleau sand (Oligocene) in the Paris Basin. Journal of Sedimentary Research, 71 (3), 473–483.

Thiry, M., Fernandes, P., Milnes, A., Raynal, J.-P., 2014. Driving forces for the weathering and alteration of silica in the regolith: implications for the studies of prehistoric flint tools. Earth-Science Reviews, 136, 141–154.

Thompson, D.L., Stilwell, J.D., Hall, M., 2015. Lacustrine carbonate reservoirs from Early Cretaceous rift lakes of Western Gondwana: Pre-Salt coquinas of Brazil and West Africa. Gondwana Research, 28, 26–51.

Torsvik, T.H., Rousse, S., Labails, C., Smethurst, M., 2009. A new scheme for the opening of the South Atlantic Ocean and the dissection of an Aptian salt basin. Geophysical Journal International, 177(3), 1315–1333.

Tosca, N.J., Wright, V.P., 2014. The formation and diagenesis of Mg-clay minerals in lacustrine carbonate reservoirs. American Association of Petroleum Geologists Search and Discovery Article #51002.

Tosca, N.J., Wright, V.P., 2015. Diagenetic pathways linked to labile Mg-clays in lacustrine carbonate reservoirs: a model for the origin of secondary porosity in the Cretaceous Pre-salt Barra Velha Formation, Offshore Brazil, 435. Geological Society of London, Special Publication. SP435-1.

Tréguet, P., Nelson, D.M., Van Bennekom, A.J., DeMaster, D.J., Leynaert, A., Quéguiner, B., 1995. The silica balance in the world ocean: A reestimate. Science, 268, 375–379.

Unternehr, P., Peron-Pinvidic, G., Manatschal, G., Sutra, E., 2010. Hyper-extended crust in the South Atlantic: in search of a model. Petroleum Geoscience, 16 (3), 207–215.

Veizer, J., Fritz, P., Jones, B., 1986. Geochemistry of brachiopods: Oxygen and carbon isotopic records of Paleozoic oceans. Geochimica et Cosmochimica Acta, 50, 1679-1696.

Von Nicolai, C., Scheck-Wenderoth, M., Warsitzka, M., Schødt, N., Andersen, J., 2013. The deep structure of the South Atlantic Kwanza Basin: insights from 3D structural and gravimetric modelling. Tectonophysics 604, 139–152.

Warren, J.K., 2016. Evaporites: A Geological Compendium (2nd edition; revised and expanded). Berlin, Springer, 1807 pp.

Wattinne, A., 2004. Evolution d'un environnement carbonate lacustre à bioconstructions, en Limagne Bourbonnaise (Oligo-Miocene, Massif Central, France). PhD Thesis, Museum National d'Histoire Naturelle de Paris, 280 pp.

Watney, W.L., Rush, J., 2012. Modeling CO_2 sequestration in saline aquifer and depleted oil reservoir to evaluate regional CO_2 sequestration potential of Ozark Plateau Aquifer System, In: South-Central Kansas, 13th Quaterly Progress Report.

White, R., McKenzie, D., 1989. Magmatism at rift zones: the generation of volcanic continental margins and flood basalts. Journal of Geophysical Research, 94, 7685–7729.

Wright, V.P., 2012. Lacustrine carbonates in rift settings: the interaction of volcanic and microbial processes on carbonate deposition. In: Garland, J., Neilson, J.E., Laubach, S.E., Whidden, K.J. (Eds). Advances in Carbonate Exploration and Reservoir Analysis. Geological Society, London, Special Publications, 370, 39–47.

Wright, V.P., Barnett, A.J., 2015. An abiotic model for the development of textures in some South Atlantic early Cretaceous lacustrine carbonates. In: Bosence, D.W.J., Gibbons, K.A., le Heron, D.P., Morgan, W.A., Pritchard, T., Vining, B.A. (Eds.), Microbial

Carbonates in Space and Time: Implications for Global Exploration and Production. Geological Society, London, Special Publications 418, pp. 209–219.

Yoshimura, J., Miyazaki, T., Wada, T., Kohra, K., 1979. Measurement of local variations in spacing and orientation of lattice plane of synthetic quartz. Journal of Crystal Growth, 46, 691–700.

Zeyen, N., Benzerara, K., Li, J., Groleau, A., Balan, E., Robert, J.-L., Esteve, I., Tavera, R., Moreira, D., Lopez-Garcia, P., 2015. Formation of low-T hydrated silicates in modern microbialites from Mexico and implications for microbial fossilization. Frontiers in Earth Sciences, 64.

Ziegler, P.A., 1992. Geodynamics of rifting and implications for hydrocarbon habitat. Tectonophysics, 215, 221–253.

Figure captions

Figure 1: (A) Location map of the studied wells and outcrops in the Congo, Kwanza, and Namibe basins (modified from Torsvik, *et al.*, 2009; Matthews *et al.*, 2011; Heine *et al.*, 2013; Seton *et al.*, 2014; Péron-Pinvidic *et al.*, 2015). (B) Palaeogeographical map of the presalt basins at the Lower Aptian (124-123 Ma) replacing the studied material in lacustrine environments (modified from Chaboureau *et al.*, 2013).

Figure 2: Schematic representation of typical diagenetic sequences (Not to scale; AC: aragonite to calcite neomorphism; Ank: ankerite; BC: blocky calcite; Cal.: calcite; Dol.: dolomite; F. BC: ferroan blocky calcite; FC to dol.: radiofibrous calcite to dolomite; FQ: fibrous microquartz; pFQ: porous fibrous microquartz; LQ: laminated microquartz; MQ: megaquartz; Ox.: oxides; Sdl.: saddle dolomite; Sdl. to Cal: saddle dolomite replaced by calcite). Major fracturing and dissolution stages are reported as *f(n)* and *d(n)* respectively. Colours of carbonates and sulphates refer to cathodoluminescence observations. Quartz cements are in blue. Notice that time is not constrained, all sequences can be considered as asynchronous.

Figure 3: Photomicrographs of Mariquita (A-E) and Mina do Gesso (F-G), onshore Kwanza Basin. (A) Cross-polarized light (XPL) view of fibrous microquartz cement (FQ) followed by megaquartz (MQ) in a calcitic matrix (Cal.) of microbial origin. (B) XPL view of botryoids of radiaxial calcite, which has been successively dolomitized (Dol.), fractured and enclosed in a megaquartz cement (MQ). (C) Plain polarized light (PLL) view of fibrous microquartz cement (FQ) followed by megaquartz (MQ). (D) XPL view of a dolomitized laminated crystalline crust that underwent fracturing and dissolution before megaquartz precipitation

(adapted from Foubert et al., 2014). (E) Location of some of the SIMS measurements in the megaquartz of Mariquita. Note the general ^{18}O enrichment through time. (F) XPL view of partial fibrous microquartz precipitation along several planes of a calcitic (Cal) spherulite (yellow arrows). (G) PPL (left) and XPL (right) of fibrous microquartz cement in the fenestral porosity of micritic microbial mats.

Figure 4: Photomicrograph and SEM pictures of Shrubby-1 (Chela Fm.), offshore Kwanza Basin. (A) PPL (left) and cathodoluminescence (CL; right) views of quartz precipitations in pores. A first generation porous fibrous microquartz (pFQ1) is followed by a thin isopachous layer of laminated microquartz cement (LQ1), and by megaquartz cement (MQ). The initial shrubs that constitute the substratum underwent several stages of dolomitization (Dol) and dissolution. (B) Close-up view of pFQ1, LQ1, and MQ under UV epifluorescence highlighting the porous nature of pFQ1 and LQ1 (blue fluorescence due to the impregnated epoxy resin). (C) Close-up view of pFQ1, LQ1, and MQ under PPL. Some patches of microquartz (μQ) occur. Notice the bitumen occurring sporadically inside the porosity of pFQ1. (D) PPL view highlighting pFQ1 and pFQ2. Notice the exceptional porosity of pFQ1 (blue due to the epoxy resin). pFQ2 has a petaloid texture and pores are filled by bitumen. (E) PPL view of length-slow fibrous microquartz determined using a first order (full wave) retardation plate. (F) SEM view of laminated microquartz cement (LQ) followed by megaquartz cements (MQ). (G) SEM view of aligned anhedral to euhedral microquartz crystals along fibers and planes of the pFQ1 fibrous cement (yellow arrows). (H) SEM view of megaquartz cement (MQ). (I) SEM element map highlighting the porous nature (dark grey) of pFQ1 and LQ1.

Figure 5: Photomicrographs of Shrubby-1 (Cuvo Fm., offshore Kwanza; A-B), Berilo (offshore Kwanza; C), Toca-1 (offshore Congo; D-E), and Toca-2 (offshore Congo; F-G). (A) PPL view of multiple megaquartz (MQ1 and MQ2) and porous laminated microquartz (LQ1) cements occurring in a fracture. The remaining porosity is partially filled by some blocky calcite (BC). (B) PPL view of LQ1, MQ1, and BC cements occurring in a fracture. (C) PPL view of brownish fibrous microquartz (FQ) and megaquartz (MQ) cements in fenestral porosity. (D) PPL view of fibrous microquartz cements (FQ) infilling primary porosity in the coquina facies of Toca-1. The pelecypod shells, underlined by yellow dashed lines, underwent dissolution of aragonite to calcite neomorphism. (E) Localization of SIMS $\delta^{18}O_{quartz}$ measurements in the FQ cements of Toca-1 under PPL view. (F and G) PPL (left) and CL (right) views of FQ and MQ cements infilling the porosity in the coquina facies of Toca-2. The yellow dashed lines underline the recrystallized and dissolved bivalve shells.

Figure 6: SIMS $\delta^{18}O_{quartz}$ (‰ SMOW) according to textural habit of quartz cements in the six studied sites. Colours of length-fast and non porous length-slow fibrous microquartz were determined according to microscopic observations using a λ-retardation plate. Colour of the microporous length-slow fibrous microquartz according to the blue epoxy resin observed in the porosity.

Figure 7: Silica solubility curves as a function of pH at 25 and 100°C, calculated using PHREEQC. Thermodynamic data come from the Thermoddem database (http://Thermoddem.brgm.fr/; Blanc *et al.*, 2012). Log K are given values at standard state conditions (T = 298 K, P = 1 atm). The log K of chalcedony has been considered as equivalent of fibrous microquartz. Log $K_{quartz(alpha)}$ = -3.740; Log $K_{chalcedony}$ = -3.456.

Figure 8: $\delta^{18}O_{quartz}$ (‰ SMOW) as a function of temperature (°C) for (A) the fibrous microquartz cements and (B) the megaquartz cements. Oxygen isotopic compositions of water (dashed lines) were calculated using the quartz-water fractionation equation of Matsuhisa *et al.* (1979): $1000\ln\alpha_{quartz\text{-}H2O} = 3.34(10^6 T^{-2})\text{-}3.31$. T, T1, T2 and T3 refer to the hypothetical minimum and maximum temperatures of crystallization (*cf*. discussion).

Figure 9: Range of $\delta^{18}O_{quartz}$ (‰ SMOW) values in the present study and comparison with values derived from a literature review of $\delta^{18}O_{quartz}$ in carbonate rocks, according to quartz morphologies and precipitation settings (A: Ewers, 1991; B: Sharp *et al.*, 2016; C: Clayton & Steiner, 1975; D: Herzig *et al*; 1988; E: Shanks *et al*., 2007; F: Renaut *et al.*, 2002; G: Saller *et al.*, 2016; H: O'Neil & Hay, 1973; I: Degens & Epstein, 1962; J: Kolodny & Epstein, 1976; K: Knauth & Epstein, 1975; L: McBride *et al.*, 1999; M: Harris, 1989; N: Abruzzese *et al.*, 2005; O: Jourdan *et al.*, 2009). Precipitation settings are defined according to the published interpretations. Laboratory techniques used for $\delta^{18}O_{quartz}$ measurements (bulk or microsampling, laser fluorination or SIMS) are specified.

Figure 10: Relative timing and proxies controlling silica cements in the presalt deposits of the West African margin, according to their petrographic and isotopic evolution. Please refer to the part 5.4 of the discussion for explanations. Colours in 3A and 3B are representative of microscope observations with a λ-retardation plate. The colour in 3B' is representative of the blue epoxy resin impregnating the microporosity of those fibrous microquartz.

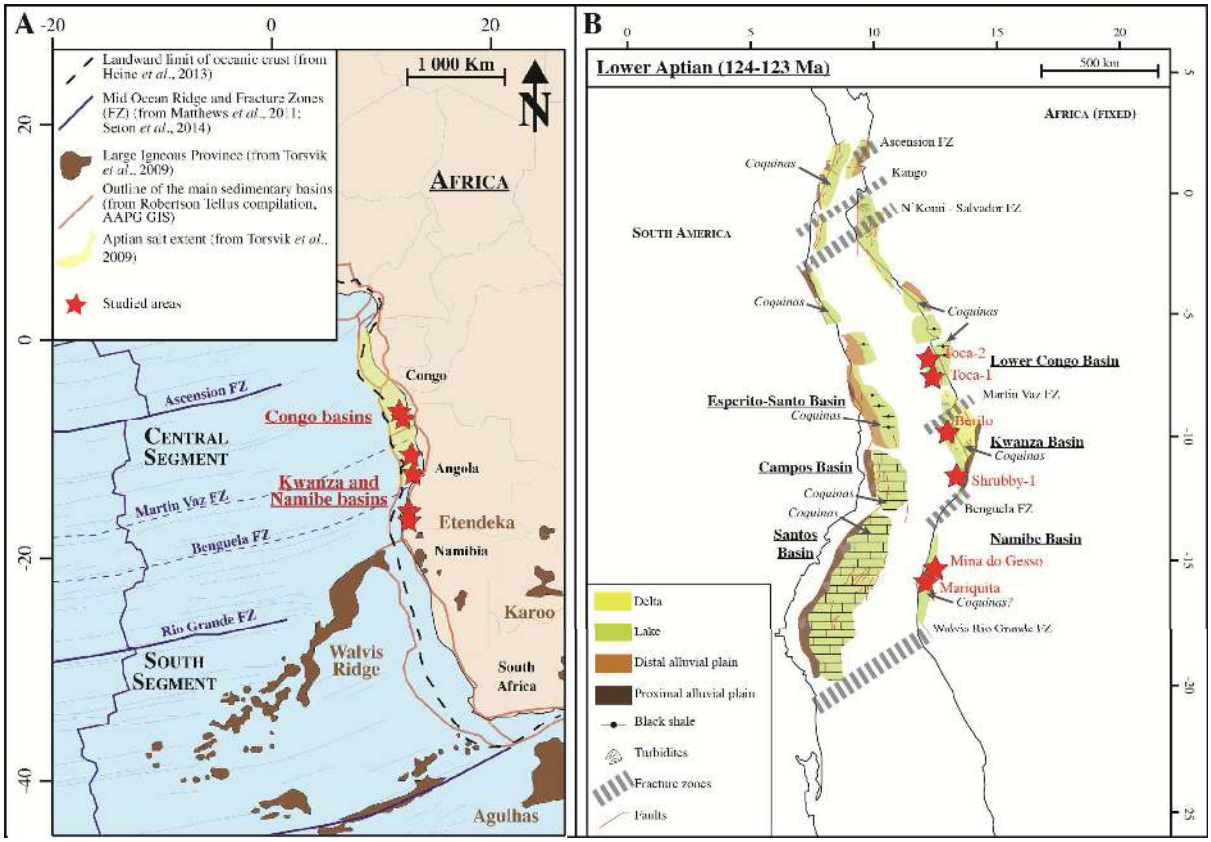
A
Landward limit of oceanic crust (from Heine et al., 2013)
Mid Ocean Ridge and Fracture Zones (FZ) (from Matthews et al., 2011; Seton et al., 2014)
Large Igneous Province (from Torsvik et al., 2009)
Outline of the main sedimentary basins (from Robertson Tellus compilation, AAPG GIS)
Aptian salt extent (from Torsvik et al., 2009)
Studied areas
1 000 Km
N
AFRICA
Congo
Angola
Namibia
Etendeka
Karoo
South Africa
Ascension FZ
Congo basins
CENTRAL SEGMENT
Kwanza and Namibe basins
Martin Vaz FZ
Benguela FZ
Rio Grande FZ
SOUTH SEGMENT
Walvis Ridge
Agulhas
B
Lower Aptian (124-123 Ma)
500 km
AFRICA (FIXED)
SOUTH AMERICA
Ascension FZ
Kongo
N'Komi - Salvador FZ
Coquinas
Toca-2
Toca-1
Lower Congo Basin
Esperito-Santo Basin
Martin Vaz FZ
Berilo
Kwanza Basin
Campos Basin
Shrubby-1
Benguela FZ
Santos Basin
Namibe Basin
Mina do Gesso
Mariquita
Coquinas?
Walvis Rio Grande FZ
Delta
Lake
Distal alluvial plain
Proximal alluvial plain
Black shale
Turbidites
Fracture zones
Faults

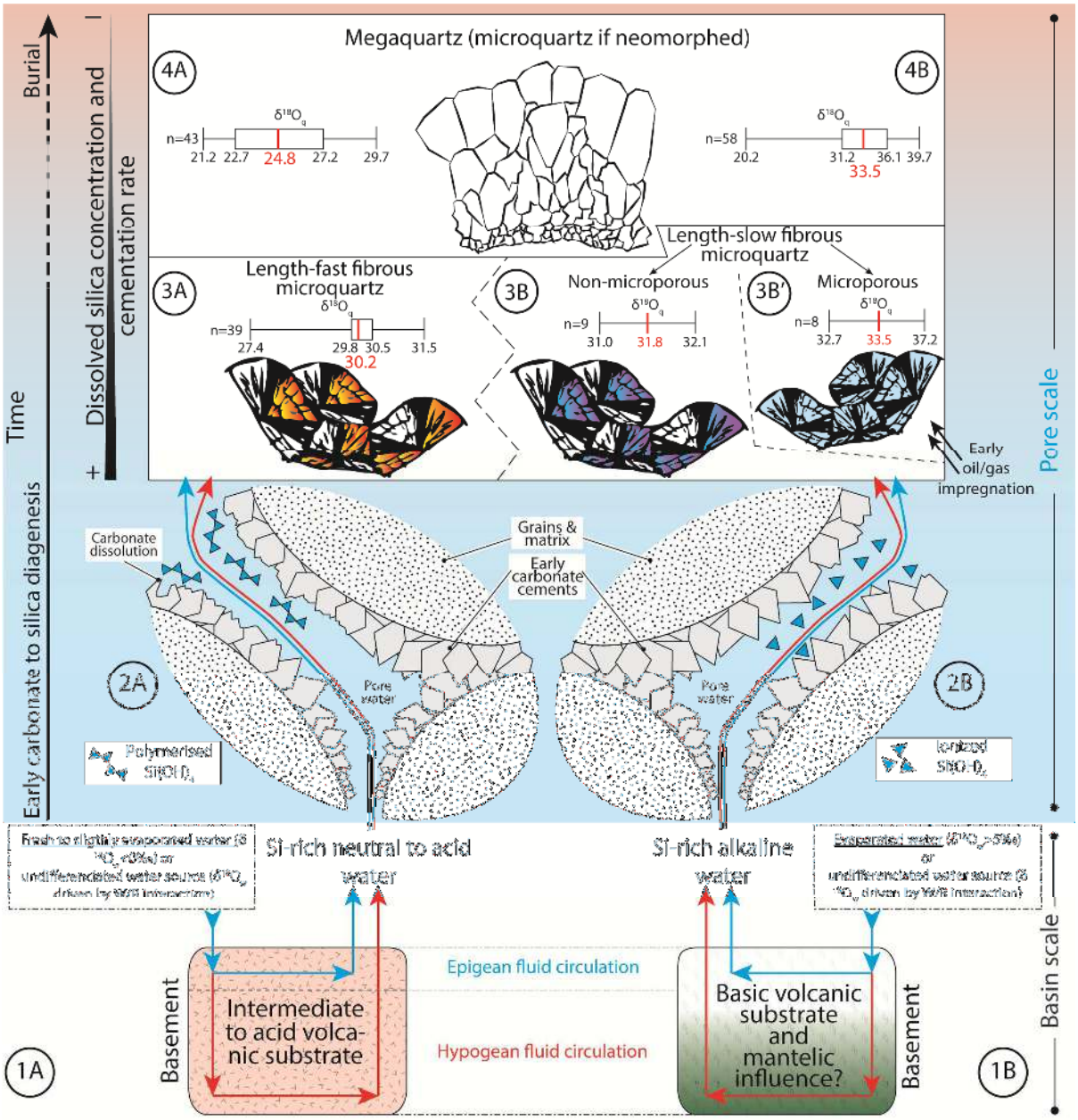
Megaquartz (microquartz if neomorphed)
4A
4B
n=43
21.2 22.7 24.8 27.2 29.7
n=58
20.2 31.2 36.1 39.7
33.5
Length-slow fibrous microquartz
3A
Length-fast fibrous microquartz
n=39
27.4 29.8 30.5 31.5
30.2
3B
Non-microporous
n=9
31.0 31.8 32.1
3B'
Microporous
n=8
32.7 33.5 37.2
Early oil/gas impregnation
Pore scale
Burial
Time
Early carbonate to silica diagenesis
Dissolved silica concentration and cementation rate
Carbonate dissolution
Grains & matrix
Early carbonate cements
Pore water
2A
2B
Polymerised SiO2
Si-rich neutral to acid water
Si-rich alkaline water
Epigean fluid circulation
Hypogean fluid circulation
Basement
Intermediate to acid volcanic substrate
Basic volcanic substrate and mantelic influence?
1A
1B
Basin scale

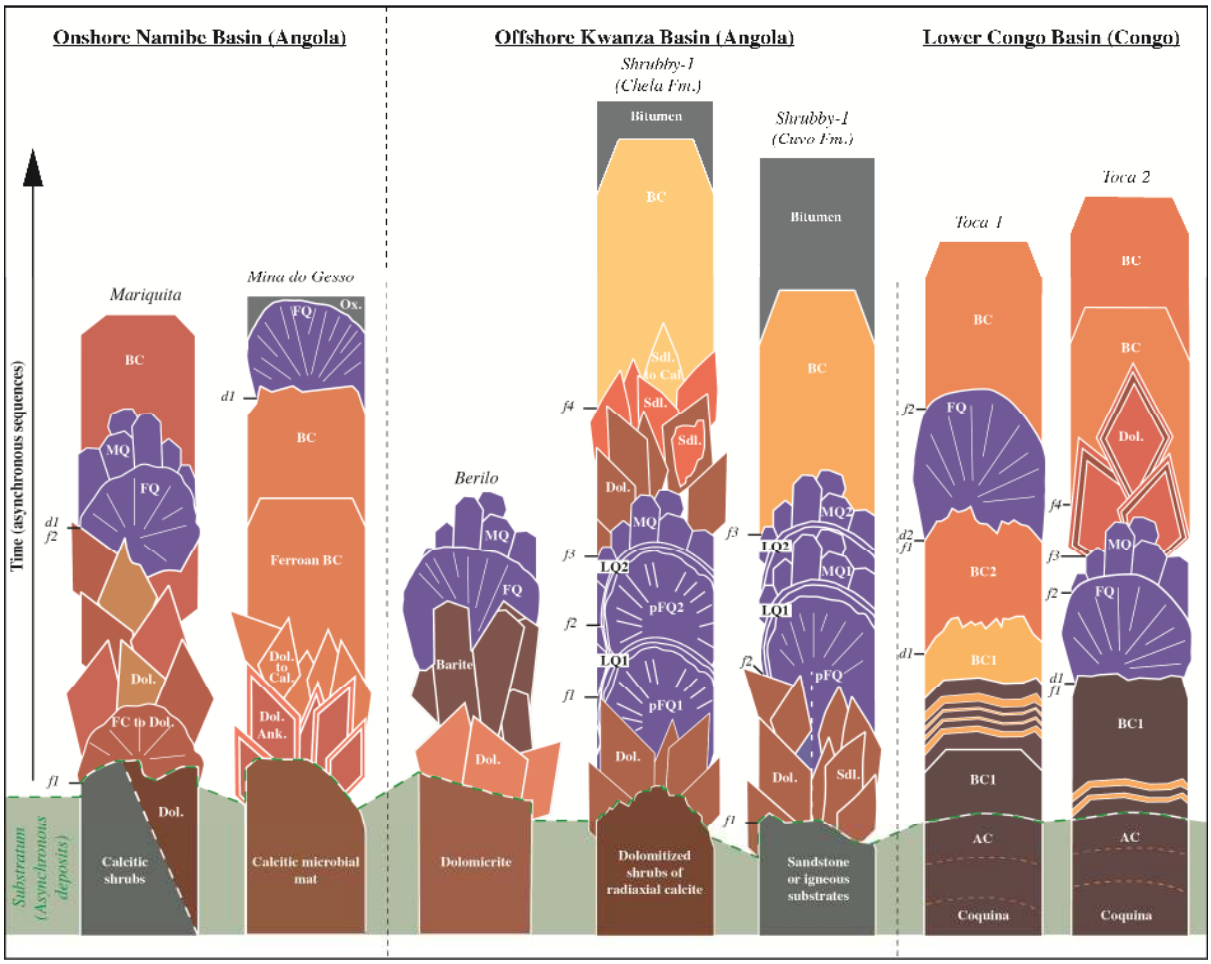
Onshore Namibe Basin (Angola)
Offshore Kwanza Basin (Angola)
Lower Congo Basin (Congo)
Time (asynchronous sequences)
Substratum (Asynchronous deposits)
Mariquita
Mina do Gesso
Berilo
Shrubby-1 (Chela Fm.)
Shrubby-1 (Cuvo Fm.)
Toca 1
Toca 2
BC
MQ
FQ
Ox.
Ferroan BC
Dol.
Dol. to Cal.
Dol. Ank.
FC to Dol.
Barite
Bitumen
Sdl.
Sdl. to Cal.
LQ2
LQ1
pFQ2
pFQ1
pFQ
MQ2
MQ1
BC2
BC1
AC
Coquina
d1
d2
f1
f2
f3
f4
Calcitic shrubs
Calcitic microbial mat
Dolomicrite
Dolomitized shrubs of radiaxial calcite
Sandstone or igneous substrates

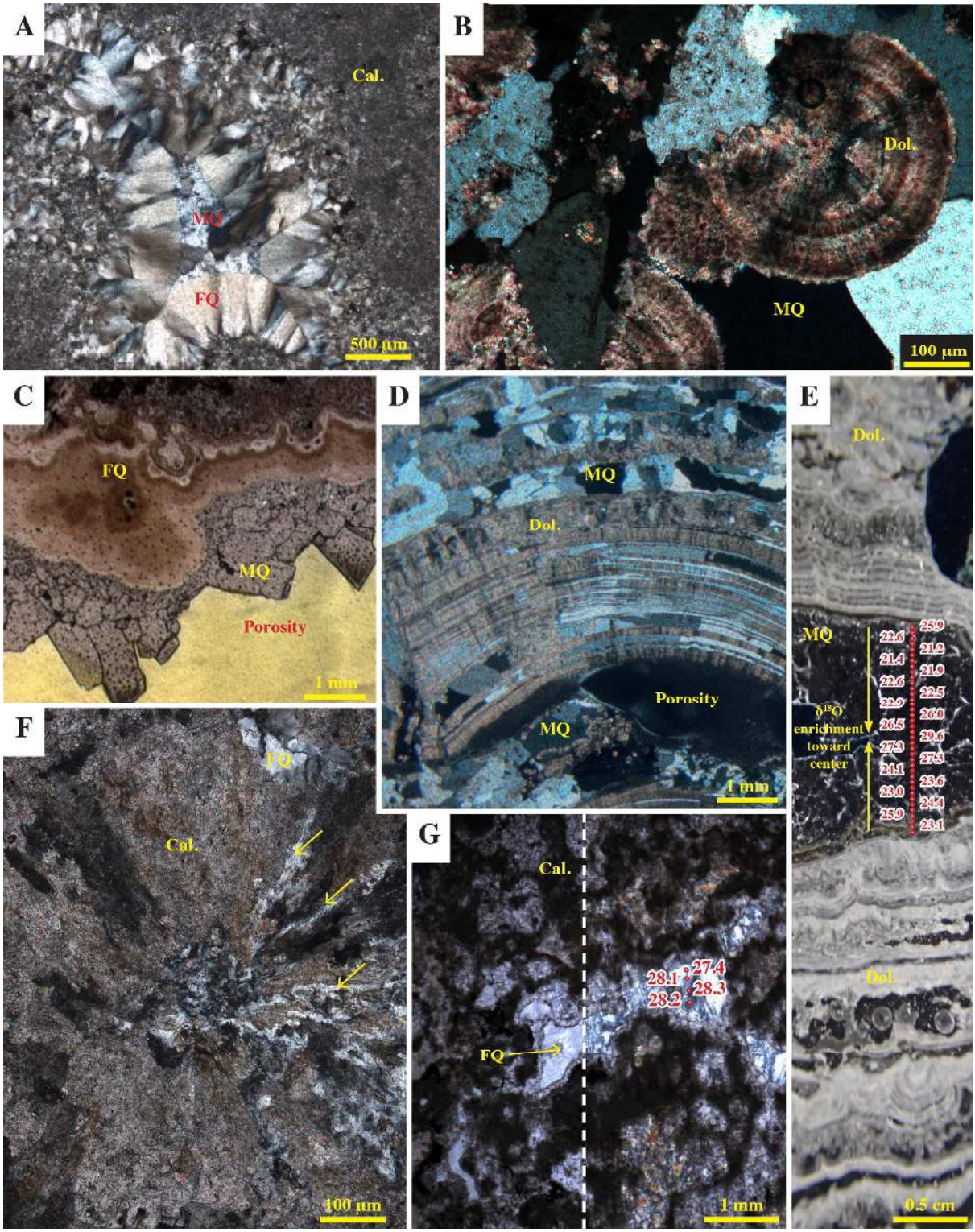
A
Cal.
MQ
FQ
500 µm
B
Dol.
MQ
100 µm
C
FQ
MQ
Porosity
1 mm
D
MQ
Dol.
Porosity
MQ
1 mm
E
Dol.
MQ
22.6
21.4
22.6
22.9
26.5
27.3
24.1
23.0
25.9
25.9
21.2
21.9
22.5
26.0
29.6
27.5
23.6
24.4
23.1
δ18O enrichment toward center
Dol.
0.5 cm
F
FQ
Cal.
100 µm
G
Cal.
28.1
27.4
28.3
28.2
FQ
1 mm

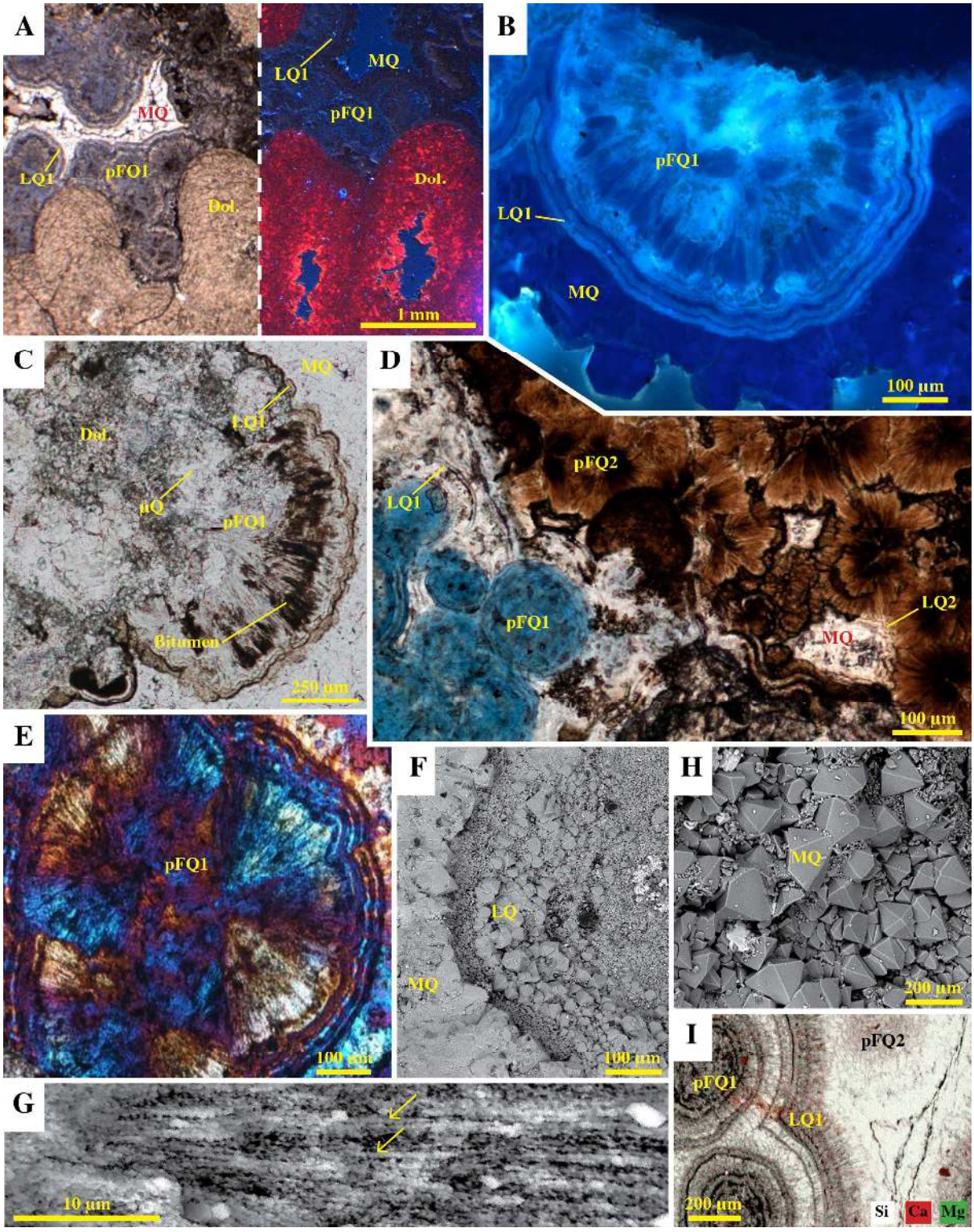
A
MQ
LQ1
pFQ1
Dol.
LQ1
MQ
pFQ1
Dol.
1 mm
B
pFQ1
LQ1
MQ
100 µm
C
MQ
LQ1
Dol.
µQ
pFQ1
Bitumen
250 µm
D
pFQ2
LQ1
pFQ1
LQ2
MQ
100 µm
E
pFQ1
100 µm
F
LQ
MQ
100 µm
H
MQ
200 µm
I
pFQ2
pFQ1
LQ1
200 µm
Si
Ca
Mg
G
10 µm

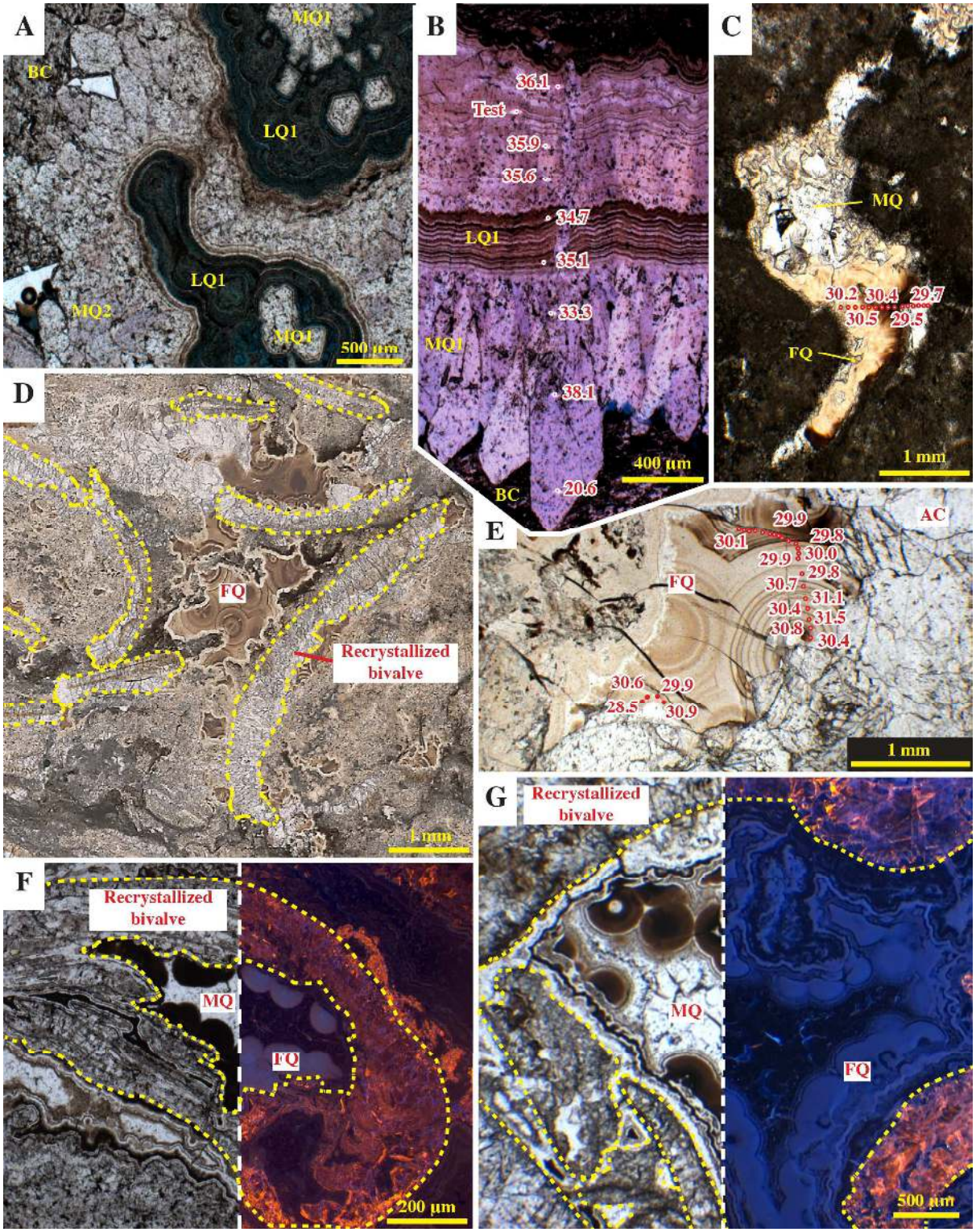
A
MQ1
BC
LQ1
LQ1
MQ2
MQ1
500 µm
B
36.1
Test
35.9
35.6
34.7
LQ1
35.1
33.3
MQ1
38.1
400 µm
BC
20.6
C
MQ
30.2
30.4
29.7
30.5
29.5
FQ
1 mm
D
FQ
Recrystallized bivalve
1 mm
E
AC
29.9
30.1
29.8
29.9
30.0
29.8
30.7
31.1
30.4
31.5
30.8
30.4
FQ
30.6
29.9
28.5
30.9
1 mm
F
Recrystallized bivalve
MQ
FQ
200 µm
G
Recrystallized bivalve
MQ
FQ
500 µm

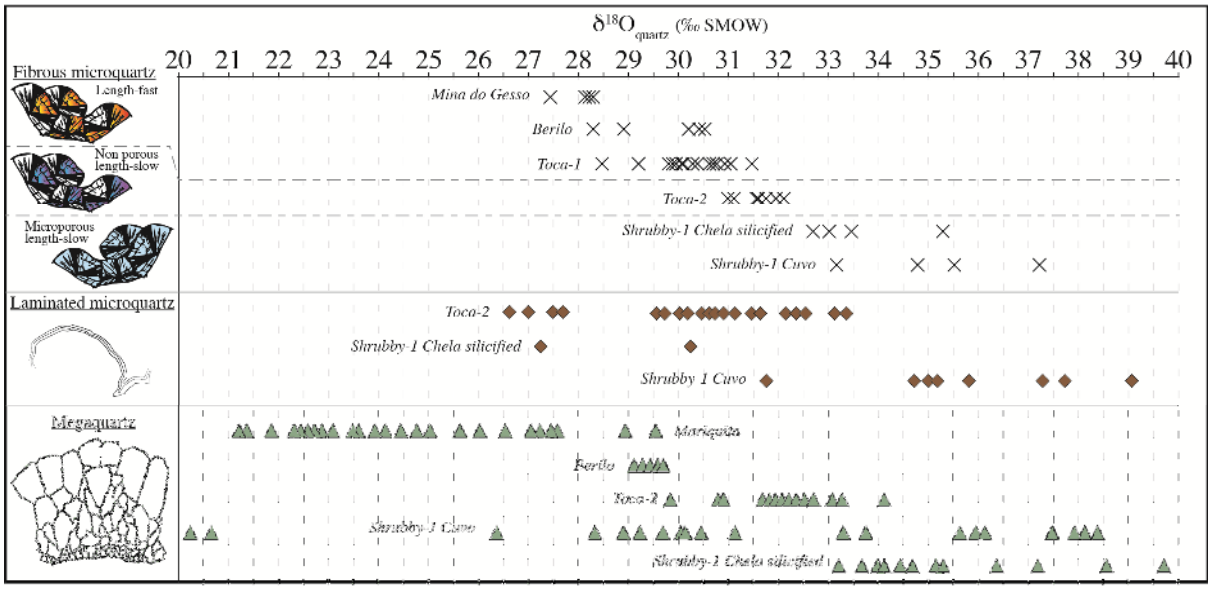
δ18Oquartz (‰ SMOW)
20 21 22 23 24 25 26 27 28 29 30 31 32 33 34 35 36 37 38 39 40
Fibrous microquartz
Length-fast
Non porous length-slow
Microporous length-slow
Laminated microquartz
Megaquartz
Mina do Gesso
Berilo
Toca-1
Toca-2
Shrubby-1 Chela silicified
Shrubby-1 Cuvo
Toca-2
Shrubby-1 Chela silicified
Shrubby 1 Cuvo
Morrinho
Berilo
Toca-2
Shrubby-1 Cuvo
Shrubby-1 Chela silicified

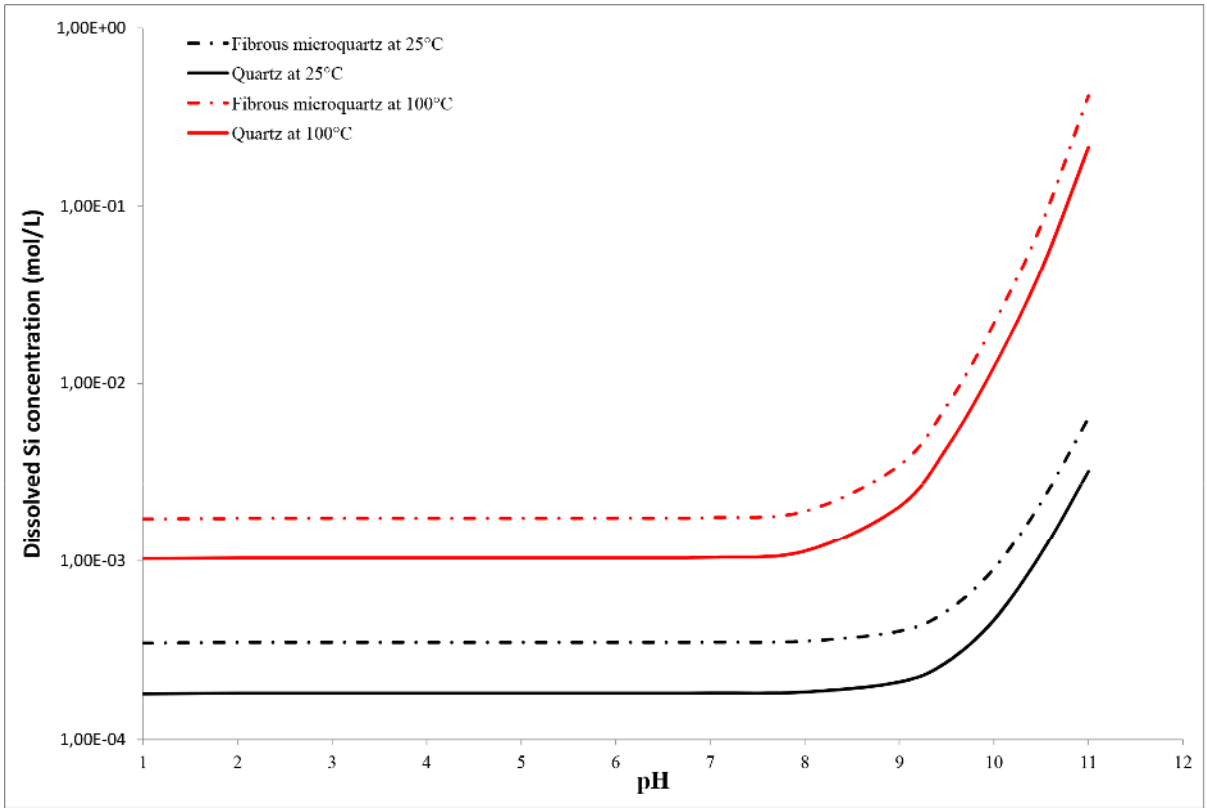
1,00E+00
1,00E-01
1,00E-02
1,00E-03
1,00E-04
Dissolved Si concentration (mol/L)
Fibrous microquartz at 25°C
Quartz at 25°C
Fibrous microquartz at 100°C
Quartz at 100°C
1
2
3
4
5
6
7
8
9
10
11
12
pH

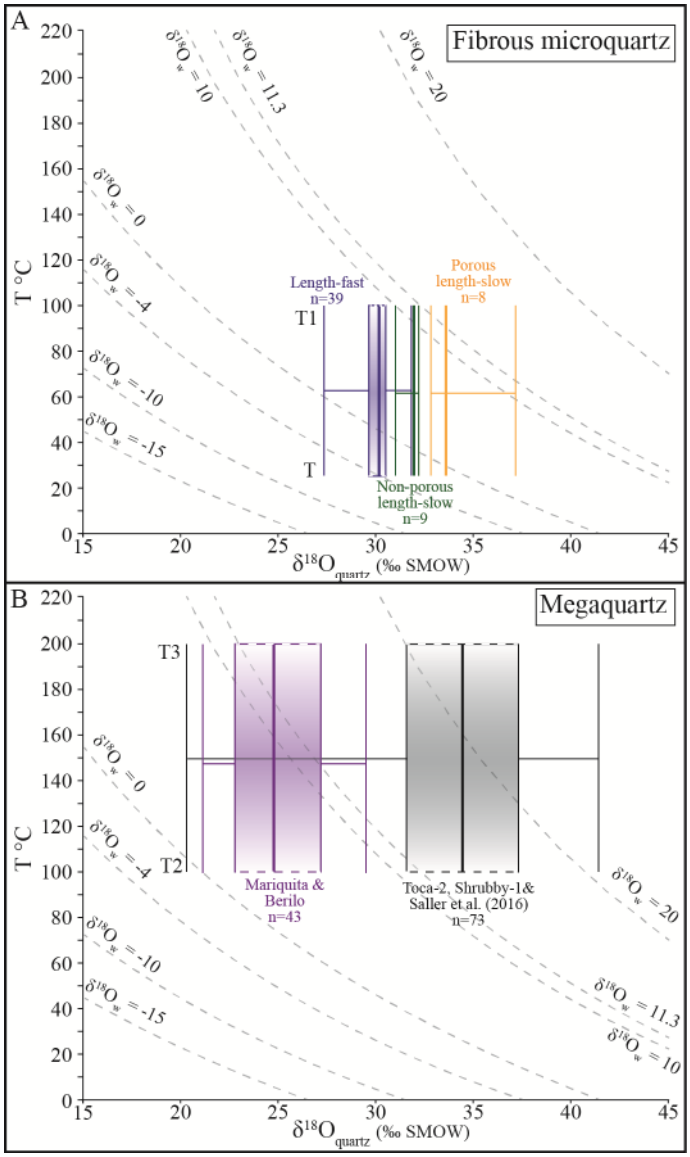
A
Fibrous microquartz
$\delta^{18}O_w = 10$
$\delta^{18}O_w = 11.3$
$\delta^{18}O_w = 20$
$\delta^{18}O_w = 0$
$\delta^{18}O_w = -4$
$\delta^{18}O_w = -10$
$\delta^{18}O_w = -15$
Length-fast
n=39
Porous
length-slow
n=8
T1
T
Non-porous
length-slow
n=9
T °C
$\delta^{18}O_{quartz}$ (‰ SMOW)
B
Megaquartz
T3
T2
Mariquita &
Berilo
n=43
Toca-2, Shrubby-1&
Saller et.al. (2016)
n=73
$\delta^{18}O_w = 0$
$\delta^{18}O_w = -4$
$\delta^{18}O_w = -10$
$\delta^{18}O_w = -15$
$\delta^{18}O_w = 20$
$\delta^{18}O_w = 11.3$
$\delta^{18}O_w = 10$
T °C
$\delta^{18}O_{quartz}$ (‰ SMOW)

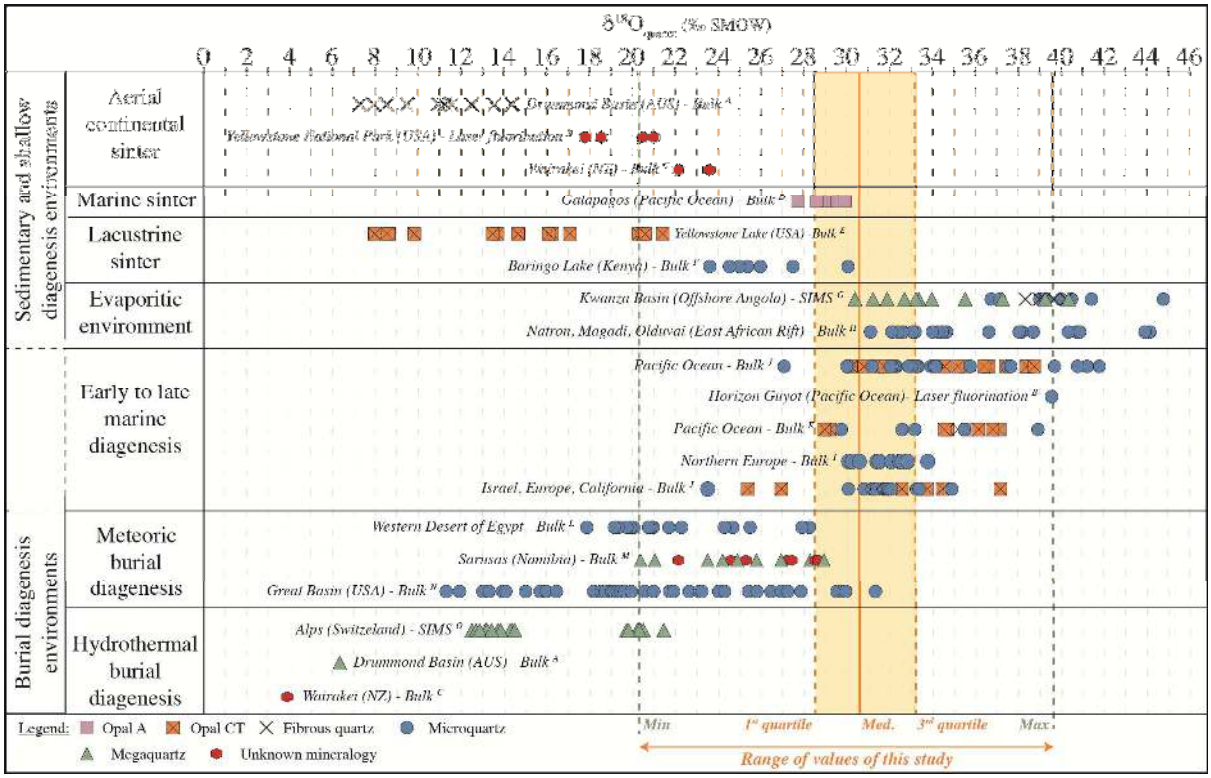
δ18Owater (‰ SMOW)
0 2 4 6 8 10 12 14 16 18 20 22 24 26 28 30 32 34 36 38 40 42 44 46
Sedimentary and shallow diagenesis environments
Burial diagenesis environments
Aerial continental sinter
Marine sinter
Lacustrine sinter
Evaporitic environment
Early to late marine diagenesis
Meteoric burial diagenesis
Hydrothermal burial diagenesis
Yellowstone National Park (USA) - Laser fluorination B
Waiotapu (NZ) - Bulk C
Galapagos (Pacific Ocean) Bulk D
Yellowstone Lake (USA) Bulk E
Boringo Lake (Kenya) - Bulk F
Kwanza Basin (Offshore Angola) - SIMS G
Natron, Magadi, Olduvai (East African Rift) Bulk H
Pacific Ocean - Bulk I
Horizon Guyot (Pacific Ocean) - Laser fluorination B
Pacific Ocean - Bulk K
Northern Europe - Bulk I
Israel, Europe, California - Bulk J
Western Desert of Egypt Bulk L
Sarusas (Namibia) - Bulk M
Great Basin (USA) - Bulk N
Alps (Switzeland) - SIMS O
Drummond Basin (AUS) Bulk A
Waiotapu (NZ) - Bulk C
Legend: Opal A Opal CT Fibrous quartz Microquartz
Megaquartz Unknown mineralogy
Min 1st quartile Med. 3rd quartile Max
Range of values of this study

- Quartz cements show extremely high $\delta^{18}O$ values (up to 40‰)
- In situ $\delta^{18}O$ analyses reveal a variability between and within different quartz generations
- $\delta^{18}O$ associated with length fast and length slow quartz habits helps to understand paleofluid history.